MODELING MICRO-DAMAGE HEALING MECHANISM AT MICRO-SCALE

A Thesis

by

MAHSA ARASTOO

Submitted to the Office of Graduate Studies of
Texas A&M University
in partial fulfillment of the requirements for the degree of

MASTER OF SCIENCE

Chair of Committee,	Dallas N. Little
Committee Members,	Mary Beth Hueste
	Ibrahim Karaman
	Harold Boas
	Masoud Darabi
Head of Department,	Robin Autenrieth

August 2013

Major Subject: Civil Enginnering

ABSTRACT

This thesis demonstrates the effect of micro-damage healing on stress and displacement fields in the vicinity of a crack tip in the material that tend to self-heal. The micro-damage healing model is modeled by incorporating time-dependent traction within the crack faces. This time-dependent traction occurs in a small zone referred to as healing process zone. The effect of the micro-damage healing on crack propagation in elastic media is investigated by deriving analytical relations for Stress Intensity Factor (SIF) when micro-damage healing mechanism is in effect. It is shown that the larger values of both healing process zone and bonding strength decrease the value of SIF near the crack tip. In order to clearly capture this phenomenon, a novel technique based on complex variables is used to derive the equations to calculate the stress and displacement fields in elastic media. Using the third correspondence principle, which is suitable in analyzing the crack shortening (healing phenomenon), the corresponding results of stress and displacement fields in elastic media are converted into viscoelastic media. Since asphalt has time-dependent material properties, the viscoelastic result is more accurate than the elastic. It is shown that an increase in the value of both healing process zone and bonding strength results in a decrease in the stress and displacement fields near the crack tip. Finally, the effect of using different coefficients in defining the bonding strength and relaxation time is evaluated.

Asphalt concrete pavements are concurrently subjected to mechanical and environmental loading conditions during their service life. Applied mechanical and

environmental loadings gradually degrade properties of asphalt concrete pavements. However, under specific conditions, asphalt concrete has the potential to heal and regain part of its strength. Identifying a model for the healing process is crucial. This proposed model is not dependent on the test methods that empower its usage in computational modeling. Moreover, this research considers both effects of instantaneous healing (a result of wetting) and time-dependent bond strength (a result of molecular diffusion between the crack faces), using the complex-variable method. Schapery (1989) considered only instantaneous healing and regarded it as the total bond strength. Therefore, considering both effects of instantaneous and time-dependent bond-strength makes this model superior with respect to the analogous model. It is hoped that this research provides insight on the healing mechanism at micro-scale.

DEDICATION

This thesis is dedicated to my family for their

Love, Support and Motivations

throughout my life.

ACKNOWLEDGMENTS

My last two years at Texas A&M University have been a great time in where I have gained a lot of experience and knowledge. This could not have been possible without the help of so many fabulous people.

I would like to thank my advisor, Dr. Little. He has been very helpful and understandable. I am thankful for his patience and support.

I would also like to thank Dr. Darabi for his time and guidance without which, this work could have never been possible. My sincere thanks go to Dr. Boas for his critical assistance when my research was stuck. Furthermore, I am very appreciative of my other committee members, Dr. Hueste and Dr. Karaman, for their helps and advices throughout this research.

My deepest gratitude goes to all of my friends and colleagues for being beside me in all good and bad moments.

I would also want to acknowledge ARC for their financial support.

Last but not least, I would like to thank my family for their encouragement, love and supports throughout my life.

TABLE OF CONTENTS

Page

LIST OF FIGURES

Page

1. INTRODUCTION

Asphalt concrete pavements are subjected to concurrent mechanical loading and environmental conditions during their service life. While traffic is considered as mechanical loading, other factors, such as moisture, temperature, and oxidation diffusion, are specified as environmental effects that impact pavement performance. Although asphalt properties degrade under the aforementioned conditions, asphalt has the ability to regain at least some of its strength under some specific conditions.

Partial or full recovery of strength or stiffness, called healing, is an intrinsic property of bitumen that leads to an improvement in the serviceability of asphalt pavements. This phenomenon can be observed within both cohesive and adhesive modes. Cohesive healing occurs in the bitumen or mastic; however, adhesive healing takes place at the bitumen–aggregate interface. Healing can be influenced by both internal factors and external factors. Physical, compositional, chemical and thermodynamic properties, such as penetration value and softening point, chemical composition, surface free energy, and volumetric properties are specified as internal factors. Factors, such as the rest periods, temperature, loading methodology, load level, damage level, compressive stress, aging, and moistures, are considered external factors.

Investigating the effect of both internal and external factors on the healing process has drawn considerable attention in recent years, largely spurred by work at Texas A&M University in the mid-1980s (Kim et al., 1990). Previously published studies have suggested that extended rest periods, can greatly improve the healing ability

of asphalt mixtures (Kim, 2003; Kim et al., 2001; Shen et al., 2010; Tan et al., 2012). However, greater levels of damage due to higher loading magnitudes or more loading cycles have proven to negatively impact healing since regions of greater damage are probably less likely to heave due to a higher gradient of molecular disturbance associated with more damage (Little et al., 2001). Moreover, higher temperature accelerates the healing mechanism (Shen et al., 2010; Williams et al., 2001).

1.1 Effect of micro-damage healing on pavement performance

Improved serviceability through healing must also reflect the potential for healing to affect the factors that impact serviceability including fatigue cracking and rutting. Results of fatigue cracking, obtained from laboratory and field experiments, do not usually match each other. Therefore the experimental results are scaled using the so-called shift factor which can be as high as 20 (Little and Bhasin, 2007). Shift factors (SF) are caused by healing (SF_h), residual stresses (SF_r) and resilient dilation (SF_d) which are expressed in Eq. (1) (Lytton et al., 1993).

$$SF = SF_h + SF_r + SF_d \tag{1}$$

The SF_h value varies between 1 and 10, while the value of SF_r changes between $\frac{1}{3}$ to 3. Finally SF_d can be as low as 1 and as high as 5. Lytton et al. investigated the importance of rest periods (i.e., healing), including both frequencies and durations, on the aforementioned healing shift factor (SF_h), such that:

$$SF_h = 1 + a(t_r)^b \tag{2}$$

where t_r is the rest period, a and b are the healing coefficient and exponent, respectively. Different rest periods result in different values of a and b. Lytton et al. (1993) attained the healing coefficients based on the field data for different climatic zones.

Eq. (2) can be expressed in more detailed format, such that:

$$SF = 1 + (\frac{n_{ri}}{N_0})a(\frac{t_r}{t_0})^h \quad (3)$$

where n_{ri} and N_0 represent the number of rest periods and cycles to fatigue failure, respectively. Moreover, t_0 and t_r express the time between cyclic load and rest period in fatigue test, respectively (Little et al., 2001).

Little et al. (2001) and Lytton et al. (2001) tried to improve the concept of shift factor by implementing the asphalt binders' healing potential, such that:

$$\frac{dh}{dN} = \text{Function}(t_r, h_1, h_2, h_\beta) \quad (4)$$

where h_1 and h_2 are the short-term and long-term healing rate, respectively, and h_β is the maximum healing achieved by the binder. Since $\frac{dh}{dN}$ (rate of healing per load cycle) has the same concept as $\frac{dC}{dN}$ (rate of cracking per load cycle) in fracture mechanics, it can be implemented in fatigue- crack modeling.

1.2 Experimental studies on the significance of micro-damage healing

Developing a model for the healing process is crucial and requires expensive and time-consuming tests. The common laboratory testing practice is to induce resting

periods among the loading cycles to investigate the changes in the material's properties before and after the rest period. Although these experiments have their own merits, conclusions might also be dependent on the test methods which restrict their usage in computational modeling. Fatigue related healing test (FH) and fracture related healing test (FRAH) are the two common lab tests used to characterize healing capabilities of asphalt concrete materials. Fatigue related healing tests are also divided into two categories: Fatigue related healing with intermittent loading (FHI) and Fatigue related healing with storage periods (FHS). In FHI tests, the intermittent loading is applied; however, in FHS tests, a continuous loading with an inserted storage period is considered. Kim and his co-workers conducted a controlled-strain dynamic mechanical analysis (DMA) test in order to understand the fatigue and healing characterization of asphalt mixtures in sand asphalt samples (Kim, 2003; Kim et al., 2001). They used a parameter, called pseudo stiffness, to estimate the effect of rest periods on healing. The experiment on the cylindrical sample, used for this torsional test, was conducted under 25C and 10 Hz. As it can be seen in Figure 1, they showed that the slope of stress-pseudo strain response at the 3000^{th} cycle is smaller than at the 80^{th} cycle, meaning that the micro damage has occurred.

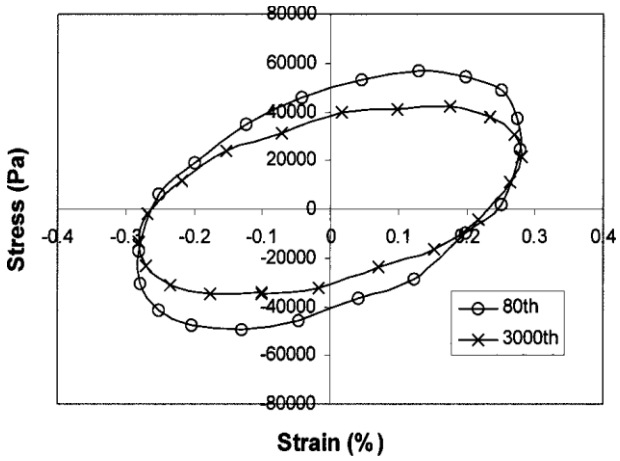

Figure 1: Stress-strain hysteresis loops and typical trend of strain-controlled fatigue tests (Kim, 2003).

A two-minute rest period is applied ten times in order to capture the micro damage healing. As it is expected, an increase in dynamic modulus is achieved after each rest period which is shown in Figure 2.

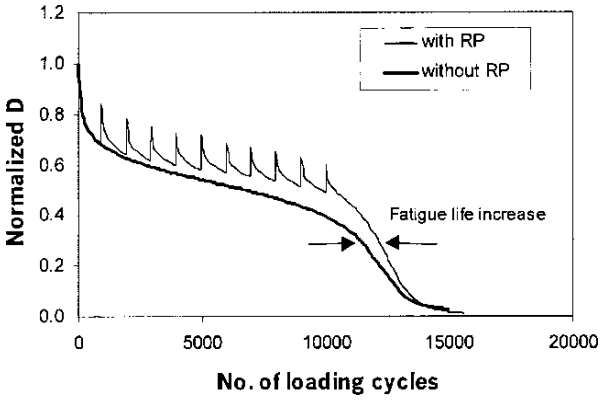

Figure 2: Normalized dynamic modulus versus number of loading cycles with and without rest periods (Kim, 2003).

Shen and her colleagues studied the effect of cohesive healing for two different types of binders named PG64-28 (neat binder) and PG70-28(polymer modified binder)

under the condition of 10 °C and 25 °C with 10 Hz. (Shen et al., 2010). Based on the result presented in Figure 3, as the rest period increases, the G* loses its value in longer loading cycles. It is also mentioned that the phase angle does not change significantly, so the G* is used as a parameter to represent deterioration in fatigue loading test. Authors also evaluate the effect of strain level and temperatures on healing in their paper.

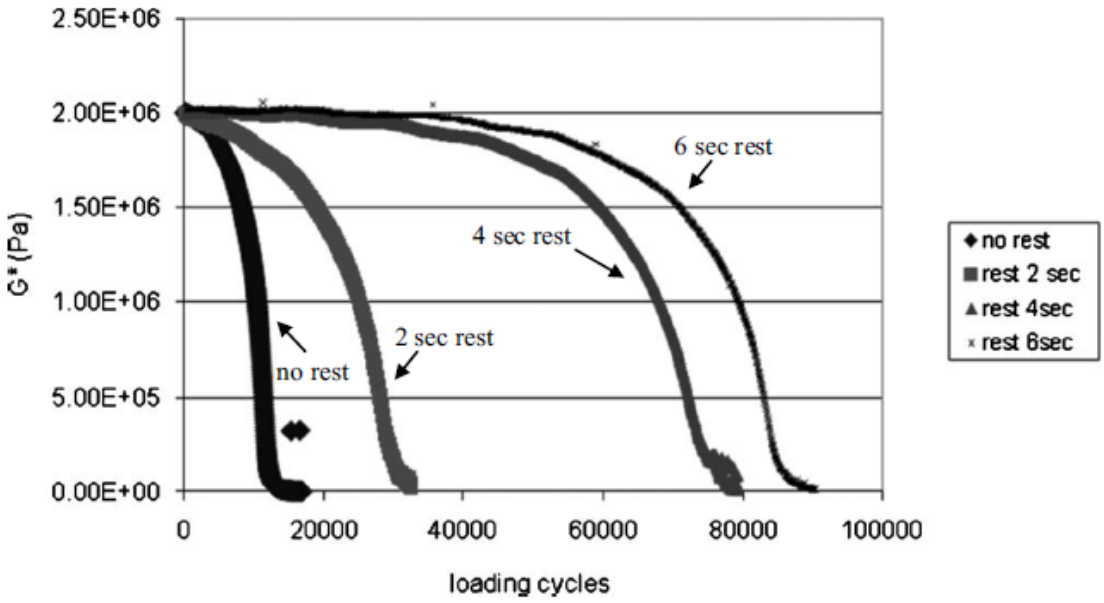

Figure 3: G* deterioration curve for the PG64-28 binder with different RPs (Shen et al., 2010).

In the FRAH, the resting period is inserted between two fracture tests. (Bommavaram et al., 2009) used this type of test for determining intrinsic healing properties of asphalt binders.

As mentioned before, the experimental results are dependent on the test methods. Therefore, finding a way to overlook this problem is essential. Some of the previous studies done in this field are outlined in the subsequent sub-sections.

These studies show the significant effect of resting time on the healing capability of asphalt concrete materials. Therefore, it is imperative to investigate the effect of resting time and different loading scenarios on the healing response of materials. This thesis tries to address this issue by mathematically illustrating stress and displacement fields, in the presence of healing effect, during a hypothetical loading-unloading scenario.

1.3 Macro-recovery parameter to characterize healing

Some materials are self-healing, meaning that a chemical and/or thermodynamic process occurs that promote a structural recovery. The self-healing mechanism can be divided into five steps according to Wool and O'Conner (Wool and Oconnor, 1981). These stages are named (a) surface rearrangement, (b) surface approach, (c) wetting, (d) diffusion, and (e) randomization. The first stage affects the topological feature of the interface while the surface approach specifies the mode for healing. Wetting stage measures the wetting function. Improvement of the mechanical property is mostly dependent on the diffusion part and at the last stage, the healing process is completed. Figure 4 shows all the stages described above.

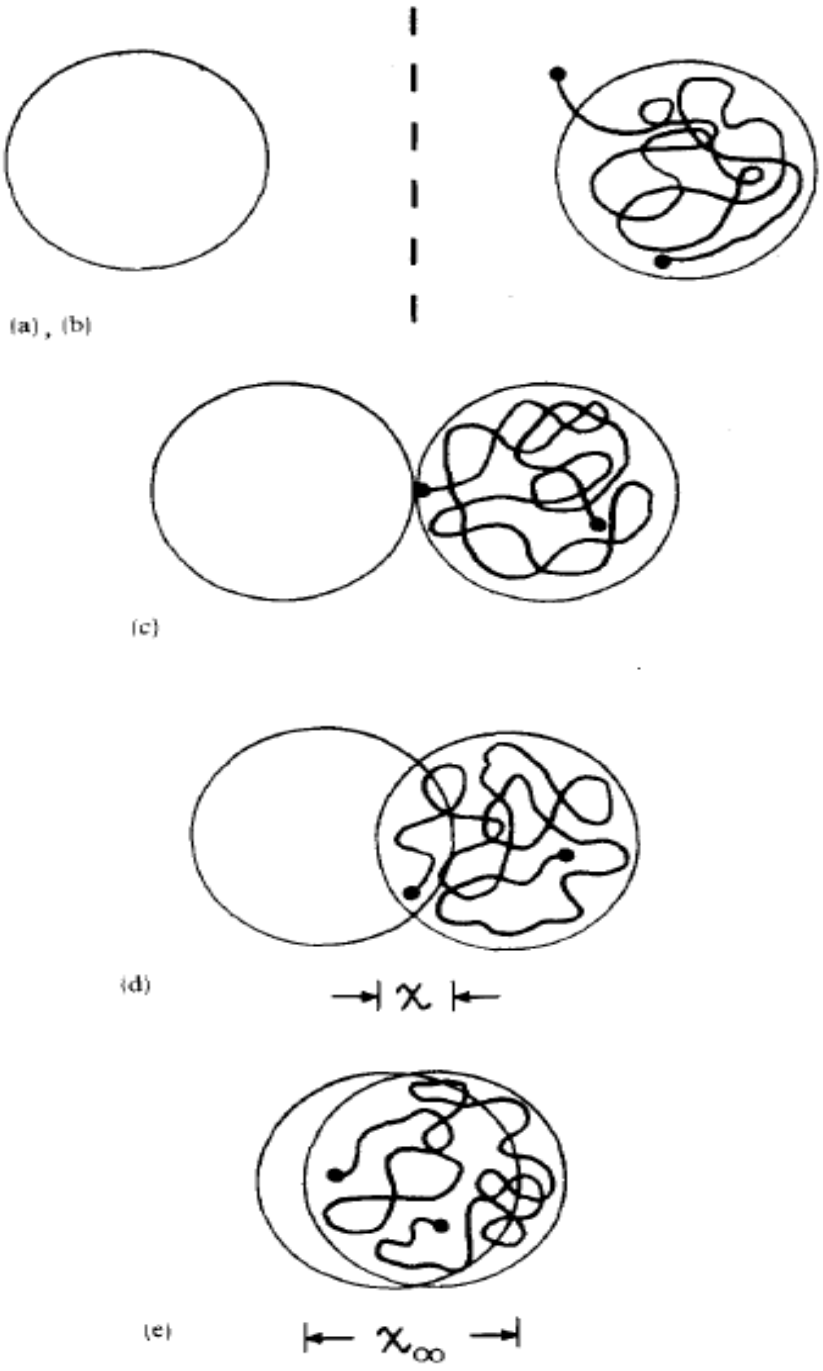

Figure 4: Five stages of healing (Wool and Oconnor, 1981).

Denoting the fracture stress by σ, the changes of stress in each stage are as follows. While in steps (a) and (b), σ has a positive value, in the wetting stage, it reaches a specific value called σ_0. The diffusion stage increases the amount of stress by σ_d, such that:

$$\sigma_d = Kt^{1/4} \tag{5}$$

where K is a constant, dependent on temperature, pressure and molecular weight. σ_d finally in the last stage reaches the fracture strength of the virgin material, called σ_∞. Also, authors conducted some experiments to show the relation between the parameters and time, molecular weight, temperature and pressure.

When two polymers contact each other at temperatures above the glass transition, the distance between them fades away and healing process begins. As discussed above, the healing process has five stages, but in this case, healing is mostly due to diffusion and randomization parts. Polymer chains cannot move freely since other chains inhibit their movements. This phenomenon is described as the Reptation model in which a chain is modeled in a tube to show the restriction caused by other chains (de Gennes, 1971). Kim proposed a theory for the last two stages of healing based on the Reptation model. (Kim and Wool, 1983). At $t = 0$, it was assumed that no chain crossed the conformation region; however, for $0 < t < T_r$, the chain started to cross the initial tube line and go through the interface as it can be seen in Figure 5. This portion of chain is called the minor chain. The fourth and fifth parts of the healing process were complete after the time T_r is reached.

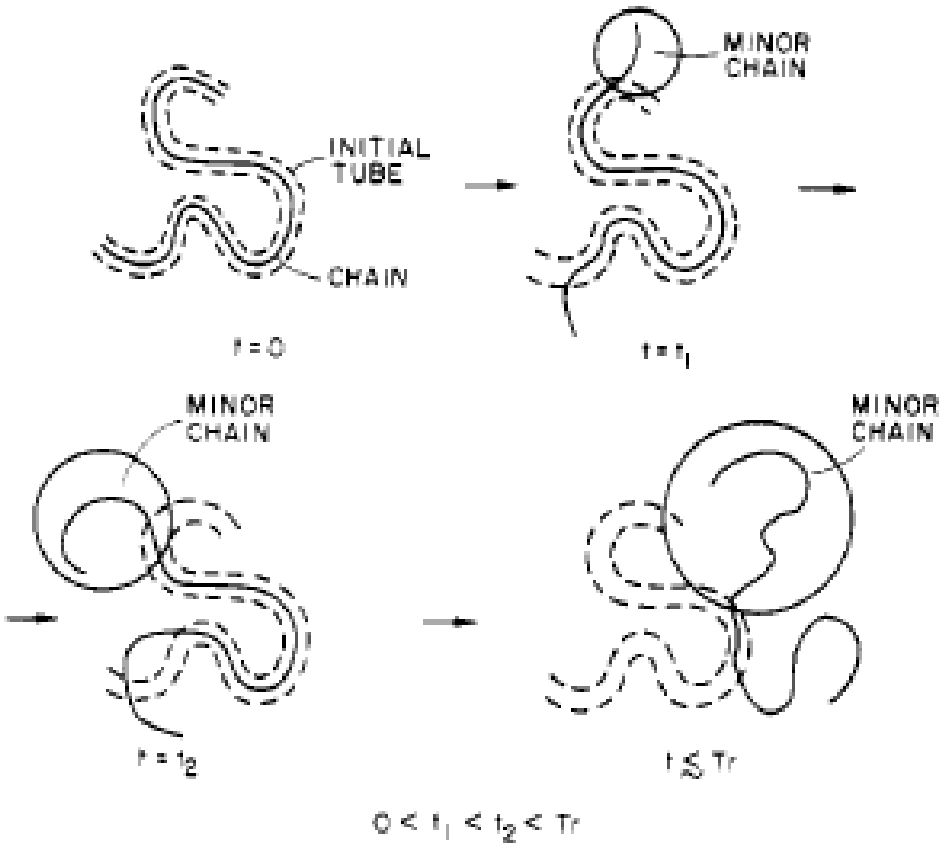

Figure 5 : Disengagement of a chain from its initial tube. The emergence and growth of minor chains are also shown (Kim and Wool, 1983).

Wool and O'Connor (1981) redefined their previous procedure to describe self-healing using two stages. In the first step, the two surfaces came into contact with each other, called wetting in which mechanical property and surface free energy were considered as important factors(i.e., considered as the combination of steps a-c in Figure 4) . Short-term and long-term strength gain, the second stage of healing, was caused by interfacial cohesion and intermolecular diffusion(i.e., considered as the combination of

d and e steps). Wool and O'Connor proposed Eq. (6) to capture the effect of both wetting and diffusion.

$$R = \int_{\tau=-\alpha}^{\tau=t} R_h(t-\tau)\frac{d\Phi(\tau)}{d\tau}d\boldsymbol{\tau} \tag{6}$$

where R shows the process of healing in all stages, R_h is the intrinsic healing function, Φ is the wetting distribution function, and τ is the time variable. As mentioned before, the higher temperature leads to a higher value of R.

Wool and O'Conner (1982) described the intrinsic healing function for stress, strain, and energy in Eqs.(7),(8) and(9).

$$R_h(\sigma,t) = \frac{1}{\sigma_\infty}\left(\sigma_0 + Kt^{1/4}\right) \tag{7}$$

$$R_h(\varepsilon,t) = \frac{1}{\varepsilon_\infty}\left(\varepsilon_0 + Jt^{1/4}\right) \tag{8}$$

$$R_h(E,t) = \frac{1}{2YE_\infty}\left(\sigma_0 + Kt^{1/4}\right)^2 \tag{9}$$

The subscript ∞ implies values measured in the virgin fracture state. J is derived via K/Y where Y is a tensile modulus. The value for E is calculated as $E = \sigma^2/2Y$, which defines the fracture energy per unit area. (Kim and Wool, 1983) conducted experiments to verify the theory in Wool and O'connor 's paper(1982).

The intrinsic healing function for polymers is presented in Eq. (10).

$$R_h(t) = R_0 + Kt^{0.25} \bullet \zeta(t) \tag{10}$$

where ζ (t) represents the surface arrangement of the molecules. The symbol $\bullet$ stands for convolution integrals. Since this model is established for a simple polymer with

short-time healing, it is not appropriate for the asphalt binders. Avrami's model was used by Bhasin and Little (2008) to propose a new formula, suitable for healings in asphalt binders, which covers both short-term and long-term strength gain in healing

$$R_h(t) = R_0 + p(1-e^{-qt^r}) \tag{11}$$

where p, q, and r are the material parameters that define the time-dependent strength gain at the interface. The term R_0, represents the short-term strength gain caused by interfacial cohesion; whereas, the term $p(1-e^{-qt^r})$ effectively captures the long-term strength gain due to intermolecular diffusion. (Bommavaram et al., 2009) presented a methodology to find these parameters for five different types of binders.

Little and Bhasin (2008) used Schapery's (1989) formulation for the rate of crack shortening along with the concept of macro-recovery parameter introduced by Wool and O'connor (1981) and related the wetting distribution as a function of fundamental properties of asphalt, such that:

$$\frac{d\Phi(t,X)}{dt} = \beta\left[\frac{1}{D_1 k_m}\left\{\frac{\pi W_c}{4\left(1-\nu^2\right)\sigma_b^2\,\beta} - D_0\right\}\right]^{-1/m} \tag{12}$$

where W_c is the work of cohesion, ν is the Poisson's ratio, σ_b is the stress at crack surfaces, β is the healing process zone, D_0, D_1 and m are creep compliance parameters, and k_m is a material constant. This equation is just applicable for the constant rate of wetting.

This thesis contributes in modeling the micro-damage healing phenomenon by incorporating the effects of both wetting and intrinsic healing mechanism on stress and displacement fields near the crack tip.

1.4 Different approaches to model micro-damage healing effect

Several researchers have introduced different indices to explain this phenomenon. Tan et al. (2012) defined two indices to clarify the concept of healing.

$$HI^1 = \left(\frac{|G^*|_{terminal}}{|G^*|_{initial}}\right)\times 100 \; ; \qquad HI^2 = \left(\frac{|G^*|_{terminal}}{|G^*|_{initial}}\right)\frac{(N_{after} - N_{before})}{N_{before}}\times 100 \quad (13)$$

where HI^1 is the healing index (modulus ratio), $G^*_{initial}$ is the initial modulus value before rest, and G^*_{after} is the initial modulus after rest; while HI^2 is a healing index (cycle number ratio) , $|G^*|_{terminal}$ is the dynamic modulus when the loading stops, N_{before} is the number of cycles when the loading stops prior to rest, and N_{after} is the number of cycles when the loading stops after the rest period. Looking into Figure 6, it is obvious that the rest period can have a significant effect on the material response, especially when applied before the failure. Most of the modulus loss is recovered over time.

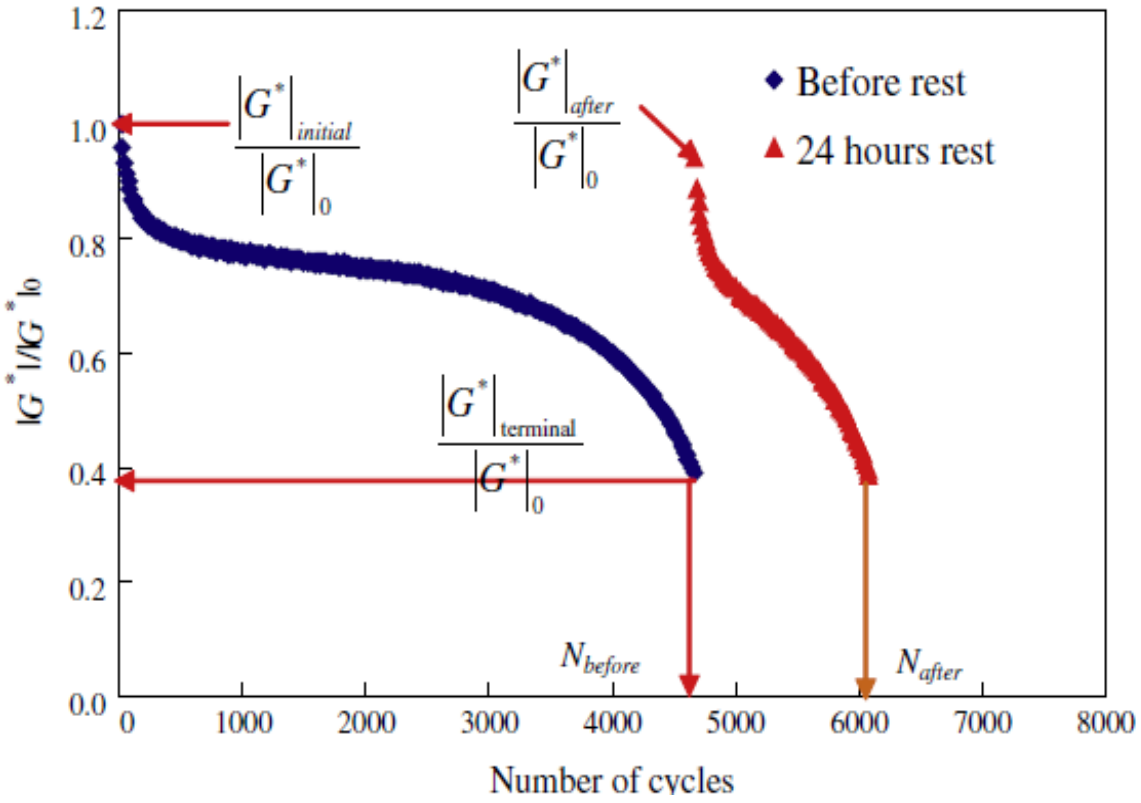

Figure 6: Schematic of fatigue indices (Tan et al., 2012).

(Little and Bhasin, 2007) defined another healing index based on the pseudo-strain energy, which was measured against different rest periods based on the experimental data of five different binders.

Another significant contribution to understand healing phenomenon was the fracture mechanics-based work of Schapery. Schapery (1989) proposed a crack shortening evolution function in viscoelastic media using the correspondence principle; however, Schapery only considered instantaneous healing to determine the rate of crack shortening. More details on Schapery's model are provided in section 2.

Although models based on fracture mechanic theories provide insight on the crack propagation and growth at micro-scale, they cannot be extended to a specimen containing considerable number of micro-cracks. Therefore, introducing a method to capture this phenomenon at macro-scale was crucial. Abu Al-Rub et al. (2010) and Darabi et al. (2012) extended the classical continuum damage mechanics framework to the continuum damage-healing framework by introducing the micro-damage healing internal state variable. They argued that the proposed framework inherits the simplicity and robustness of the well-known continuum damage mechanic theories (e.g. (Kachanov, 1958)). They proposed a phenomenological-based micro-damage healing evolution function and applied it to predict the effect of micro-damage healing on the mechanical response of bituminous materials. Further explanation is provided in section 3.

This research enhances Schapery's work by considering both effects of intrinsic and time-dependent bond strength using complex-variable method. This model mathematically demonstrates the effect of micro-damage healing on the stress intensity factor (SIF), displacement field, and stress field near the crack tip in the elastic media. Using the third correspondence principle, the result of stress and displacement fields in elastic media can be transformed into viscoelastic media. It is observed that an increase in the value of bonding strength and healing process zone will result in a decrease in the both stress and displacement field. In the last step, the effect of different relaxation time and bonding strength is evaluated.

2. FRACTURE MECHANICS

This chapter presents the fundamental concepts of fracture mechanic theories. Although considering the interactions between multiple cracks is a baffling task using fracture mechanics theories, they can be used effectively to understand the mechanism of crack nucleation, growth, and propagation at micro-scale.

2.1 Different modes of fracture

The stress distribution near the crack tip can be divided into three different categories: Mode I, Mode II and Mode III. A crack will open perpendicularly to its surface in the first mode (i.e. the stress induced is compression or tension). Mode II produces in-plane shear stress and Mode III induces anti-plane shear stress. Figure 7 schematically displays different modes of fracture.

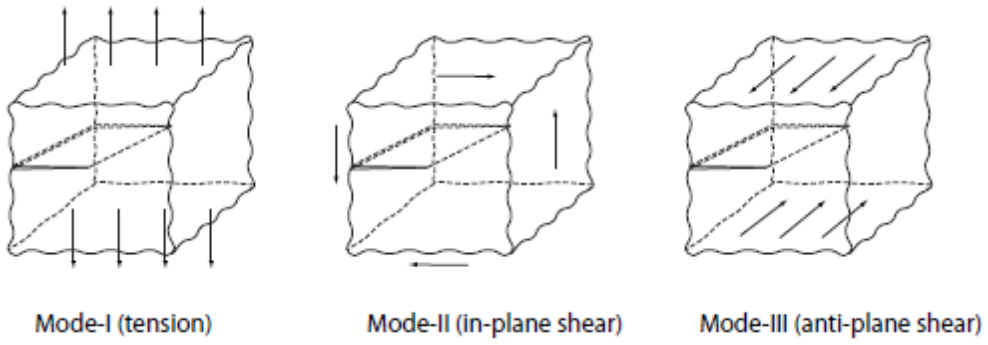

Figure 7: Different modes of fractures in a particle near the crack tip (Zehnder, 2012).

These three modes are also known as opening mode, sliding mode and tearing mode, respectively. The actual load applied to the crack could be the combination of these three modes. Both corresponding stress and displacement fields for all three Modes

are determined in the literature; however, only the first mode is investigated in this thesis.

2.2 Stress intensity factor and energy release rate

Onset of crack propagation can be defined using two different concepts: energy release rate and stress intensity factor. Griffith (1921) was the first who investigated crack nucleation and growth using fracture mechanics. He assumed an elliptical shape for the crack. Based on Griffith's criterion, crack propagation requires a sufficient amount of released energy during the crack growth. This criterion is expressed in mathematical expression as follows (Broek, 1986),

$$\frac{d}{da}(U - F + W) = 0 \Rightarrow \frac{d}{da}(F - U) = \frac{d}{da}W \tag{14}$$

where U, F, and W are elastic energy contained in the plate, work of the external force, and energy for crack formation, respectively. Moreover, a defines the length of the crack. The right hand side of Eq. (14) is the crack resistance force, R, and the left hand side states the energy release rate (crack extension force), denoted by G.

Suppose there is a plate with an internal crack, subjected to load P in perpendicular direction of crack. The work done by the external load is $Pd\nu$ where $d\nu$ represents the change in displacement. Under the assumption of linear elastic relation between displacement and loading ($\nu = CP$), elastic energy can be calculates as:

$$U = \frac{1}{2}CP^2 \tag{15}$$

Substituting Eq. (15) into Eq.(14), the energy release rate can be found, such that:

$$G = \frac{1}{2B}(P^2 \frac{\partial C}{\partial a}) \tag{16}$$

where B is the plate thickness.

Dugdale (1960) showed that the stress field near the crack tip can theoretically reach infinity in an elastic media containing a single centered crack. To characterize the stress field near the crack tip, he proposed the concept of the Stress Intensity Factor (SIF) in order to remove the singularity and to define a measure that can be used to compare stress fields near the cracks with different geometries. The SIF in opening mode (mode 1) is denoted by K_I and is expressed as:

$$K_I = \lim_{x \to 0} \left[\sigma(x) \sqrt{2\pi x} \right] \tag{17}$$

where x is the distance from the crack tip. It can be shown that for a crack with the length of $2a$ subjected to far field stress of σ_∞^R, K_I can be expressed as:

$$K_I = \sigma_\infty^R \sqrt{\pi a} \tag{18}$$

Fracture toughness is the material property which shows the resistance of the crack to fracture, denoted by K_{IC}. In a situation where the value of K_I is greater than K_{IC}, the crack will propagate.

The relations between the energy release rate and stress intensity factor for plane stress and plane strain conditions are presented in Eqs.(19) and (20), respectively.

$$G_I = \frac{K_I^2}{E} \tag{19}$$

$$G_I = (1 - \nu^2) \frac{K_I^2}{E} \tag{20}$$

where subscript I refers to the first mode of fracture and K_I is the stress intensity factor.

(Dugdale, 1960) also assumed the material behaves in an elastic-perfectly plastic mode. With the presence of plastic zone, the stress is bounded at the tip with no singularity. This requires that $K_I^R = 0$ for the fictitious crack, by which the plastic zone size and the displacement at the crack tip can be determined (Hellan, 1985).

Many studies were done to improve the work of (Griffith, 1921). He determined the breaking stress for both case of plane strain and plane stress by considering the surface energy of the crack and an increase in the strain energy caused by the crack in brittle solid. However, his formulation was not applicable to ductile materials. Orowan (1954) and Irwin (1957) tried to generalize Griffith's criterion. Barenblatt (1959a; 1959b; 1962) also worked on the equilibrium cracks in his studies (i.e., dimension of the crack does not change under the given load). In his calculation, he divided the crack into inner and outer regions. In the inner region, the displacement of the lower and upper parts of the crack is considerable; therefore, their forces can be negligible. However, in the outer region, the forces are significant, but the displacement is not. He claimed that a specific minimum force is required for the creation of the crack. After the crack reaches this state, even a small increase in the applied force could result to a sudden rupture. The mathematical theory of equilibrium cracks formed in brittle fracture is expressed in Eq. (21).

$$\sigma = \frac{N}{\sqrt{s}} + \text{a finite quantity} \tag{21}$$

where s and N shows the distance of a point to the crack boundary and stress density coefficient, respectively. (Mueller, 1971) also studied in this field.

2.3 Stress and displacement fields using complex variable method

Many studies focus on the stress distribution in the vicinity of the cracks. One solution is to assume a stress function and check whether it satisfies the equilibrium equations and boundary condition (Williams, 1957, 1959). Stress field is expressed in Eq.(22)

$$\sigma_{11} = \Phi_{,22}; \quad \sigma_{22} = \Phi_{,11}; \quad \sigma_{12} = \Phi_{,12} \tag{22}$$

where Φ is the stress function. Stresses obtained from Eq. (22) already satisfy the equilibrium equations. In order to satisfy the compatibility equations, the stress function must satisfy the biharmonic equation as indicated in Eq. (23).

$$\nabla^4 \Phi = 0 \tag{23}$$

The next step is to use the boundary conditions of the crack to find the stress function. The displacement field is the integral form of strain, obtained from the stress-strain law; however, this method is complicated due to the mathematical calculations. Williams (1957) used direct relationships between the displacement field and stress function.

Besides the airy stress function approach (described in Eq. (22)), some studies used complex variables to determine the stress field near the crack. (Hellan, 1985; Sedov, 1972)

As can be clearly seen in Figure 8, the coordinates of the crack are defined using $x_1 \equiv x$ (in the direction of the crack) and $x_2 \equiv y$ (perpendicular to the surface of the crack).

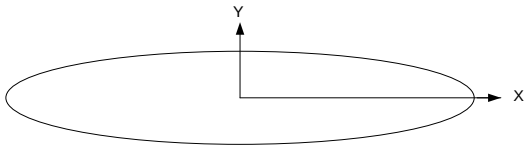

Figure 8: Schematic illustration of the crack direction.

The parameter z is expressed by Eq. (24).

$$z = x + iy \tag{24}$$

where $i = \sqrt{-1}$. Using the complex variable technique, Westergard (1939) defined the stress and displacement fields in the vicinity of the crack, such that:

$$\sigma_{11} = \mathrm{Re}\,\phi' - y\,\mathrm{Im}\,\phi'' \tag{25}$$

$$\sigma_{22} = \mathrm{Re}\,\phi' + y\,\mathrm{Im}\,\phi'' \tag{26}$$

$$\sigma_{12} = -y\,\mathrm{Re}\,\phi'' \tag{27}$$

$$u_1 = \frac{1}{2G}\left(\frac{k-1}{2}\mathrm{Re}\,\phi - y\,\mathrm{Im}\,\phi'\right) \tag{28}$$

$$u_2 = \frac{1}{2G}\left(\frac{k+1}{2}\mathrm{Im}\,\phi - y\,\mathrm{Re}\,\phi'\right) \tag{29}$$

where the value of k is $3-4\nu$ for plane strain and $\frac{3-\nu}{1+\nu}$ for plane stress. Im and Re shows the corresponding imaginary and real part of that value. The ϕ' function in mode I is calculated by Eq. (30), proposed by Sedov(1972).

$$\phi_I' = \frac{1}{\pi\sqrt{z^2 - a^2}} \int_{-a}^{a} \frac{g_2(\xi)\sqrt{a^2 - z^2}}{z - \xi} d\xi \tag{30}$$

where g_2 shows the traction loading on the surface of the crack in the x_2 direction and a defines the half length of a crack. The stress and displacement fields are planned to be calculated near the crack; therefore, the coordinate $y = 0$ is used in the computation. Eqs. (26) and (29) simplify to Eqs. (31) and (32), respectively.

$$\sigma_{22} = \mathrm{Re}\,\phi' \tag{31}$$

$$u_2 = \frac{1}{2G}\left(\frac{k+1}{2}\,\mathrm{Im}\,\phi\right) \tag{32}$$

A detailed procedure is explained in section 4.

2.4 Boltzman superposition and rate of crack shortening

(Schapery, 1975) conducted another pertinent research on crack closing and bonding in linear visco elastic media. Before going through the details of Schapery's paper, some basic concepts in visco elastic media must first be presented.

Boltzmann's superposition principle implies that the sum of the strain output resulting from each component of stress input is the same as the strain output resulting from the combined stress input. This principle is also valid for the stress field (i.e., the sum of the stress output resulting from each component of strain input is the same as the stress output resulting from the combined strain input.) (Findley et al., 1989)

Assume that a constant stress σ_1 is applied at $t = \xi_1$ then $\sigma(t) = \sigma_1 H(t - \xi_1)$ where $H(t)$ is a Heaviside unit function. If the stress input varies with time instead of being constant, it can be approximated by the sum of a series of constant stress input, described

by $\sigma(t) = \sum_{i=1}^{r} \Delta\sigma_i H(t-\xi_i)$. A corresponding strain for constant stress can be written in the form of $\varepsilon(t) = \sum_{i=1}^{r} \Delta\sigma_i H(t-\xi_i) D(t-\xi_i)$ where $D(t)$ represents the creep compliance. When the number of steps turns to infinity, summation changes into integral as expressed in Eq.(33).

$$\varepsilon(t) = \int_0^t H(t-\tau) D(t-\tau) d\sigma(\tau) \tag{33}$$

Since dummy variable τ is always less than or equal to t, $H(t-\tau)$ always equals one. Therefore Eq. (33) converts to Eq. (34).

$$\varepsilon(t) = \int_0^t D(t-\tau) \frac{\partial\sigma(\tau)}{\partial\tau} d\tau \tag{34}$$

Using the same procedure, when ε is constant and σ is a function of time, the following equation can be derived

$$\sigma(t) = \int_0^t E(t-\tau) \frac{\partial\varepsilon(\tau)}{\partial\tau} d\tau \tag{35}$$

where $E(t)$ is the relaxation modulus. With the help of Laplace transformation, Eq. (36) shows the relationship between creep and relaxation tests.

$$\int_0^t E(t-\tau) \frac{\partial D}{\partial\tau} d\tau = \int_0^t D(t-\tau) \frac{\partial E}{\partial\tau} d\tau = 1 \tag{36}$$

The correspondence principle in linear viscoelastic theory relates the stress and displacement fields in elastic and viscoelastic media using Laplace transform (i.e., the

viscoelastic solution can be constructed based on the elastic solution). Three different correspondence principles are used for different cases (Schapery, 1984).

2.4.1 CP- I

The first correspondence principle is valid for time-independent surfaces. The boundary condition is described as follows.

$$\sigma_{ij}^{R} n_j = T_i^{R} \quad \text{on } S_T; \quad u_i^{R} = U_i^{R} \quad \text{on } S_U \tag{37}$$

S_T and S_U show the boundary with prescribed traction and prescribed deformation, respectively. In this case, the viscoelastic solution is expressed in Eq. (38) and (39).

$$\sigma_{ij} = \left\{ E d\sigma_{ij}^{R} \right\} = \frac{1}{E_R} \int_{-\infty}^{t} E(t-\tau) \frac{\partial \sigma_{ij}^{R}}{\partial \tau} d\tau \tag{38}$$

$$u_i = \{ D du_i^{R} \} = E_R \int_{-\infty}^{t} D(t-\tau) \frac{\partial u_i^{R}}{\partial \tau} d\tau \tag{39}$$

where σ_{ij} and u_i are the stress and displacement fields in the viscoelastic problem; however, σ_{ij}^{R} and u_i^{R} satisfy equations in the reference elastic problem.

2.4.2 CP- II

The second correspondence principle is applicable when $\frac{dS_T}{dt} \geq 0$ (i.e., when the crack growth is being modeled). The boundary conditions considered in this case are:

$$\sigma_{ij} n_j = T_i \quad \text{on } S_T; \quad u_i = U_i \quad \text{on } S_U \tag{40}$$

In this case, the viscoelastic solution is expressed in Eqs. (41) and (42).

$$\sigma_{ij} = \sigma_{ij}^{R} \tag{41}$$

$$u_i = \{Ddu_i^R\} = E_R \int_{-\infty}^{t} D(t-\tau)\frac{\partial u_i^R}{\partial \tau} d\tau \tag{42}$$

2.4.3 CP- III

The third correspondence principle is applicable when $\frac{dS_T}{dt} \le 0$ (i.e., when the crack closing is being modeled). The concept of healing is also classified in this type of correspondence principle. The boundary conditions considered here are:

$$\sigma_{ij}^R n_j = T_i^R \quad \text{on } S_T; \quad u_i^R = U_i^R \quad S_U \tag{43}$$

In this case, the viscoelastic solution is expressed in Eqs. (44) and (45) .

$$\sigma_{ij} = \{Ed\sigma_{ij}^R\} \tag{44}$$

$$u_i = u_i^R \tag{45}$$

Returning to CP-III, the elastic problem is defined by the three major equations. First, standard equilibrium equation, which is expressed by $\partial\sigma_{ij}^R / \partial x_j + F_i^R = 0$. Second, strain-displacement equation, which is defined by $\varepsilon_{ij}^R = \frac{1}{2}(\partial u_i^R / \partial x_j + \partial u_i^R / \partial x_i)$ and finally, stress-strain equations, which is determined by $\varepsilon_{ij}^R = \left[(1+\nu)\sigma_{ij}^R - \nu\delta_{ij}\sigma_{kk}^R\right] / E_R$. Additionally, the boundary conditions were defined in Eq. (43).

Forces and tractions are different in viscoelastic and elastic problems; however, the corresponding elastic problem is found using convolution integrals as expressed in Eqs. (46) and (47).

$$T_i^R \equiv \{DdT_i\} = E_R \int_{-\infty}^{t} D(t-\tau)\frac{\partial T_i}{\partial \tau}d\tau \tag{46}$$

$$f_i^R \equiv \{Ddf_i\} = E_R \int_{-\infty}^{t} D(t-\tau)\frac{\partial f_i}{\partial \tau}d\tau \tag{47}$$

The viscoelastic boundary value problem is defined by the field equations expressed in Eqs. (48) to (50).

$$\partial\sigma_{ij} / \partial x_j + F_i = 0 \tag{48}$$

$$\varepsilon_{ij} = \frac{1}{2}(\partial u_i / \partial x_j + \partial u_i / \partial x_i) \tag{49}$$

$$\varepsilon_{ij} = \left[(1+\nu)\{Dd\sigma_{ij}\} - \nu\delta_{ij}\{Dd\sigma_{kk}^R\}\right] / E_R \tag{50}$$

The boundary conditions are also defined in Eq. (51).

$$\sigma_{ij}n_j = T_i \quad \text{on } S_T; \quad u_i = U_i \quad S_u \tag{51}$$

Schapery (1989) restricted his research to the opening mode and he neglected the effect of two other modes. Figure 9 schematically shows the stress and displacement near the crack tip in which parameters a and β define the half-crack length, and the distance in which two surfaces have a bond to each other, respectively. This bonding strength is defined by σ_b (Schapery, 1975).

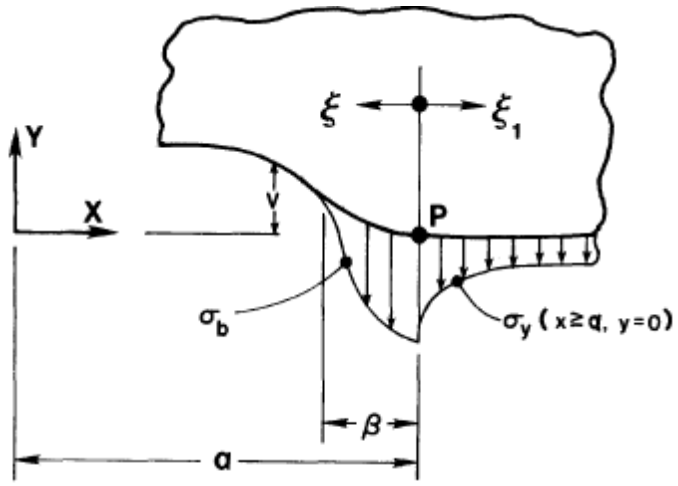

Figure 9: Bonding strength and displacement near the crack tip (Schapery, 1989).

The opening displacement *v* is obtained from CP-III.

$$v = C_R \int_0^{\beta} \sigma_b^R(\xi') F(\frac{\xi'}{\xi}) d\xi', \tag{52}$$

where $F(\frac{\xi'}{\xi}) \equiv \frac{2}{\pi}\left[2(\frac{\xi}{\xi'})^{1/2} - \ln\left|\frac{1+(\frac{\xi'}{\xi})^{1/2}}{1-(\frac{\xi'}{\xi})^{1/2}}\right|\right]$ and $C_R \equiv (1-\nu^2)/E_R$.

The stress counterpart normal to the surface in the elastic problem, called σ_b^R, is solved by Eq. (53).

$$\sigma_b^R = \{D d\sigma_b\} = E_R \int_{-\infty}^{t} D(t-\tau)\frac{\partial \sigma_b}{\partial \tau} d\tau \tag{53}$$

The stress singularity which is removed by the Barenblatt, results Eq.(54) for stress intensity factor in elastic media. The procedure was fully explained by (Schapery, 1975).

$$K_I^R = (\frac{2}{\pi})^{1/2} \int_0^{\beta} \sigma_b^R(\xi) \xi^{-1/2} d\xi \tag{54}$$

Stress and displacement fields near the crack tip are caused by both external loads and failure stress. First, the corresponding stress and displacements due to the loads with zero σ_f are considered. Second, none zero failure stress without loading is determined. Therefore the total result will be the summation of effects gained from both categories.

(Williams, 1957) found the corresponding stress and displacement equations based on considering external loads. Since the measurements are restricted to the vicinity of point P, mentioned in Figure 9, some simplifications were made on the original equations. Shortened equations are expressed in Eqs. (55) and (56).

$$\sigma_x^0 = \sigma_y^0 = [K_I / (2\pi\xi_1)^{1/2}] H(\xi_1) \tag{55}$$

$$\nu_0 = C_e [K_I / (2\pi)^{1/2}] \xi^{1/2} H(\xi) \tag{56}$$

where $C_e = 4\frac{1-\nu^2}{E}$. Young's modulus and Poisson's ratio are denoted by E and ν, respectively. (Barenblatt, 1962) also found a way to calculate the results for the failure stress.

$$\nu^f = -(C_e / 2\pi) H(\xi) \int_0^{\alpha} \sigma_f(\xi') \ln[(\xi'^{1/2} + \xi^{1/2}) / (\xi'^{1/2} - \xi^{1/2})] d\xi' \tag{57}$$

$$\sigma_x^f = \sigma_y^f = -\pi(\xi_1)^{-0.5} \int_0^{\alpha} [\sigma_f(\xi) / (\xi^{0.5})] d\xi + \sigma_f(0) + O(\xi_1^{0.5}) \tag{58}$$

As mentioned before, the total stress of the crack tip will be the summation of Eqs.(55) and (58) . In order to have a finite value of stress at the crack tip, the stress intensity factor should be calculated.

Schapery assumed a time-independent value for σ_b which is spatially uniform over $0 < \xi < \beta$. The work per unit surface area done on the particle by σ_b is $\sigma_b \nu_b$ where ν_b is the displacement at $\xi = \beta$. He defined bond energy, $2\Gamma_b$, by adding the work of the upper and lower surface of the crack.

Creep compliance is assumed to be equal to $D(t) = D_0 + D_1 t^m$, where D_0, D_1 and m are positive constant and $0 < m \leq 1$. Therefore, the reference bonding stress is expressed in Eq. (59).

$$\sigma_b^R = E_R \sigma_b \left[D_0 + D_1 (1-\eta)^m (\beta / \dot{a}_b)^m \right] \tag{59}$$

where $\eta = \xi / \beta$. Finally, the stress intensity factor is calculated in Eq. (60).

$$K_I^R = (8/\pi)^{1/2} E_R \sigma_b \beta^{1/2} \left[D_0 + D_1 \gamma_m (\beta / \dot{a}_b)^m \right] \tag{60}$$

Where γ_m is found using $\gamma_m \equiv (\pi/4)^{1/2} \Gamma(1+m) / \Gamma(1.5+m)$. Also $\Gamma(.)$ is the gamma function. The Beta function, defined by $B(x,y) = \int_0^1 t^{x-1}(1-t)^{y-1} dt$ is used for deriving the above equations. Also beta function and gamma function are related through Eq. (61).

$$B(x,y) = \frac{\Gamma(x)\Gamma(y)}{\Gamma(x+y)} \tag{61}$$

Based on previous explanation, Schapery finds the work done in Eq. (62).

$$W_b \equiv \sigma_b v_b = \frac{4}{\pi}(1-\nu^2)\sigma_b^2 \beta \left[D_0 + D_1 c_m \gamma_m (\beta / \dot{a}_b)^m \right] \tag{62}$$

where $c_m = (2m+1)/(m+1)$. Total surface energy is equal to the work done by both upper part and lower part.

Using some mathematical manipulations, normalized bonding zone length and bonding speed are expressed in Eqs. (63) and (64) .

$$\beta / \beta_m = Z(1+\lambda)^{-2} c_m^2 \tag{63}$$

where $\beta_m \equiv \pi \Gamma_b' / 2\sigma_b^2 (1-\nu^2) D_0^+ c_m^2$.

$$\dot{a}_b / \dot{a}_m = Z(1+\lambda)^{-2} \lambda^{-(1/m)} c_m^{(2+1/m)} \tag{64}$$

where $\dot{a}_m \equiv \beta_m (D_1 \gamma_m / D_0 c_m)^{1/m}$.

Parameter λ and Z are defined in Eq. (65) and (66).

$$\lambda = 0.5 \left[c_m Z + (c_m Z)^{1/2} (c_m Z + 4/c_m - 4)^{1/2} \right] - 1 \tag{65}$$

$$Z \equiv (K_I^R / K_{I0}^R)^2 \tag{66}$$

where $(K_{I0}^R)^2 \equiv 4\Gamma_b' D_0^+ (E_R^+)^2 / (1-\nu^2)$.

For different values of m , Schapery plotted the normalized displacement and normalized speed versus Z parameter which was defined in Eq. (66).

The theory is also extended to more general creep compliance defined by $D(t) = D_0 + \Delta D(t)$ where D_0 is the initial compliance. Schapery also found an upper and lower limit for stress intensity factor in his paper.

Fracture mechanics seems to be a starting point for understanding the process of crack initiation and growth; however, in order to capture the impact of all the damages

caused to the specimen by cracks, the method of continuum damage mechanics must be used. In the next section, basic concept in continuum damage mechanics is discussed.

The core concept behind this research is based on the fracture mechanics. The idea, illustrated by Schapery, is extended by considering both effect of instantaneous and time-dependent bond strength. Moreover, the concept of correspondence principle III, which was fully explained in this section, is used to transform the stress and displacement fields in elastic media into viscoelastic media.

3. CONTINUUM DAMAGE HEALING MECHANICS

Introducing a method to capture the effects of an array or system of cracks in a specimen is crucial. Therefore, the concept of continuum damage mechanics (CDM) was introduced. This chapter briefly demonstrates CDM but the main focus is on the works done to extend this concept to continuum damage healing mechanics (CDHM).

3.1 Describing different configurations in CDM

Kachanov (1958) introduced the concept of effective (undamaged) configuration; however, his idea needed to be revised in order to capture the behavior of materials with healing ability. Darabi et al. treat micro-damage healing as the reduction of the damaged area and damage density(Abu Al-Rub et al., 2010; Westergaard, 1939). In their model the cross section is divided into three different parts, represented by undamaged (effective) area, unhealed crack area, and area where micro-cracks and micro-voids are healed. Figure 10 shows the above explanation in the schematic way. It is assumed that the area with completely healed micro-cracks reaches the same property as the undamaged area.

Eq. (67) can be expressed based on explanation in Figure 10.

$$A = \bar{A} + A^D = \bar{\bar{A}} + A^{uh} \tag{67}$$

where A, $\bar{A}$, and $\bar{\bar{A}}$ are the cross-sectional area in the damaged (nominal), undamaged (effective) and healing configuration, respectively. The damaged area consists of two different parts, explained in Eq.(68).

$$A^D = A^{uh} + A^h \tag{68}$$

where A^{uh} and A^{h} represent the healed micro cracks and unhealed micro cracks, respectively.

Since loads are not carried by the unhealed micro cracks, Eq. (69) is written as a relation between nominal and healed configuration.

$$\sigma A = \bar{\bar{\sigma}} \bar{\bar{A}} \tag{69}$$

where σ and $\bar{\bar{\sigma}}$ illustrate the stress in nominal and healing configuration, respectively. (Abu Al-Rub et al., 2010) define two parameters in Eq.(70) to demonstrate other relations between damaged and healed configurations.

$$\Phi = \frac{A^D}{A}; \qquad h = \frac{A^h}{A^D} \tag{70}$$

where Φ and h are the damage variable and healing variable, respectively. Using these parameters, the relations between stresses in the aforementioned three configurations are derived as follows.

$$\bar{\sigma} = \frac{\sigma}{1-\Phi(1-h)}; \qquad \bar{\sigma} = \bar{\bar{\sigma}} \frac{1-\Phi(1-h)}{1-\Phi} \tag{71}$$

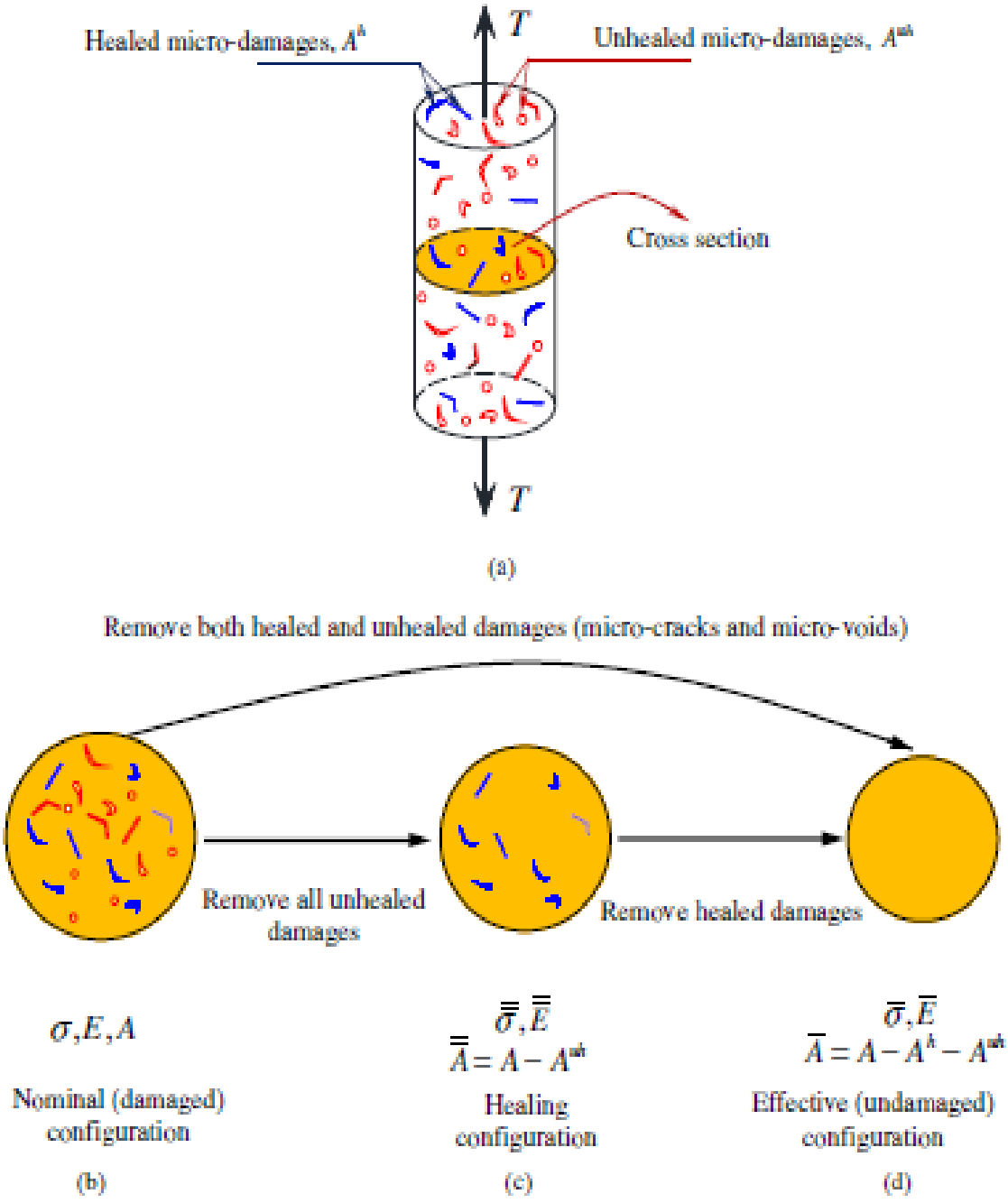

Figure 10: Schematic representation (Westergaard, 1939)

3.2 Different hypotheses to relate strain in different configurations

The thermodynamic based micro-damage healing model can be based on three different hypotheses in order to obtain the correlation between strains in the damaged and healed configurations. Eq. (72) is applicable between undamaged and healed strain for all three hypotheses.

$$\bar{\varepsilon} = \bar{\bar{\varepsilon}} \frac{1-\Phi(1-h)}{1-\Phi} \tag{72}$$

where $\bar{\varepsilon}$ and $\bar{\bar{\varepsilon}}$ are the corresponding strains in undamaged and healed configurations.

A brief discussion on these three hypotheses, called strain equivalence hypothesis, elastic strain energy equivalence hypothesis and power equivalence hypothesis, is presented in the subsections that follow.

3.2.1 Strain equivalence hypothesis

While this is the simplest transformation hypothesis, it is not applicable in large deformations or significant damage development. Equivalency in strain tensors in both nominal and healing configurations is the basis of this hypothesis which leads to a relation between the tangent stiffness moduli in nominal and healing configurations, as expressed in Eq. (73).

$$D = [1-\varphi(1-h) + (\dot{\varphi}h + \varphi\dot{h} - \dot{\varphi})\varepsilon\dot{\varepsilon}^{(-1)}]\ (\bar{\bar{D}}) \tag{73}$$

where D and $\bar{\bar{D}}$ are tangent stiffness moduli in nominal and healing configuration, respectively. Both nonlinear response and changes in the stiffness moduli are captured by this equation.

3.2.2 Elastic strain energy equivalence hypothesis

This hypothesis considers equivalent elastic strain energy for both nominal and healing configuration. Eq. (74) shows the relation of tangent stiffness moduli in nominal and healing configuration.

$$D = [[1-\varphi(1-h)]^2 + 2(\dot{\varphi}h + \varphi\dot{h} - \dot{\varphi})(1-\varphi(1-h))\varepsilon\dot{\varepsilon}^{(-1)}] \ (\bar{\bar{D}}) \tag{74}$$

3.2.3 Power equivalence hypothesis

Eq. (75) demonstrates the relation of tangent stiffness moduli in nominal and healing configuration for power equivalence hypothesis.

$$\begin{aligned} D = {} & [[1-\varphi(1-h)]^2 + (\dot{\varphi}h + \varphi\dot{h} - \dot{\varphi})(1-\varphi(1-h))\varepsilon\dot{\varepsilon}^{(-1)} - \\ & (\dot{\varphi}h + \varphi\dot{h} - \dot{\varphi})[\int_0^t (\dot{\varphi}h + \varphi\dot{h} - \dot{\varphi})\varepsilon dt]\dot{\varepsilon}^{(-1)}](\bar{\bar{D}}) \end{aligned} \tag{75}$$

While the difference between Eqs. (74) and (75) is negligible in case of low rate of healing and damage, Eq. (75) is more accurate to use.

3.3 Thermodynamic framework

The thermodynamic framework for modeling of the micro-damage healing is discussed by Darabi et al.(1939). All equations are written based on the elastic behavior and all the virtual motions are assumed to be independent. The effects of components in both internal and external power are discussed in Darabi's paper. As damage increases, the internal power increases; however, when healing occurs, the internal power decreases. This reduction in the value of internal power is the result of free energy of the cracks or an increase in configurational entropy. Both conjugate damage force and healing force are decomposed into two parts namely energetic and dissipative. The

Energetic part shows the capability of energy storage in a material and is measured by Helmholtz free energy. On the other hand, the dissipative part shows how energy dissipates in the material which can be measured by the rate of energy dissipation.

4. MICRO-DAMAGE HEALING AT MICRO-SCALE

4.1 Introduction

This research enhances Schapery's (1989) evolution function for the rate of crack closure by considering the effects of instantaneous healing and time-dependent bond strength (Wool and O'Conner (1982; 1981)). The model presented in this research mathematically illustrates the effect of micro-damage healing on the stress intensity factor (SIF), displacement field, and stress field near the crack tip. The concept of Schapery's correspondence principle III is used to transform the displacement and stress fields, determined in elastic media, to viscoelastic media. Moreover, the effect of two different parameters, bonding strength coefficient and relaxation time, on bonding strength is also evaluated.

4.2 Effect of micro-damage healing on stress intensity factor (SIF)

It is necessary to recall some key formulations on SIF that were fully described in section 2. Dugdale (1960) proposed the concept of the stress intensity factor in order to remove the singularity and to define measures that can be used to compare stress fields near the cracks with different geometries. The SIF in the opening mode (mode1) is denoted by K_I and is expressed as:

$$K_I = \lim_{x \to 0} \left[\sigma(x) \sqrt{2\pi x} \right] \tag{76}$$

where x is the distance from the crack tip. It can be shown that for a crack with the length of $2a$ subjected to far field stress of σ_∞^R, K_I can be expressed as:

$$K_I = \sigma_\infty^R \sqrt{\pi a} \tag{77}$$

Consider an infinite plate containing a centered crack of length $2a$. The plate is under the far field stress σ_∞^R in the direction perpendicular to the crack. In the absence of a healing process zone, crack faces are traction free. However, when the healing mechanism is in effect, crack faces are subjected to the bond strength σ^R. Figure 11 schematically illustrates the far field stress applied to the mode I crack and the induced bond strength within the healing process zone.

4.2.1 Elastic media- Considering constant bonding strength

The problem at hand is to determine the stress intensity factor (SIF) for a mode I crack in the presence of the micro-damage healing mechanism.

Figure 12 shows a quarter of the plate containing a mode I crack since the symmetric boundary conditions are applied. To solve this problem, the superposition principle is used. Since the material is assumed to behave linearly elastic, use of the superposition principle is valid. Therefore, the problem shown in Figure 12(a) is decomposed to the following sub-problems:

1- Far field stress applied to the plate containing a centered crack in Figure 12(b).

2- Induced bond strength within the healing process zone is considered in Figure 12(c).

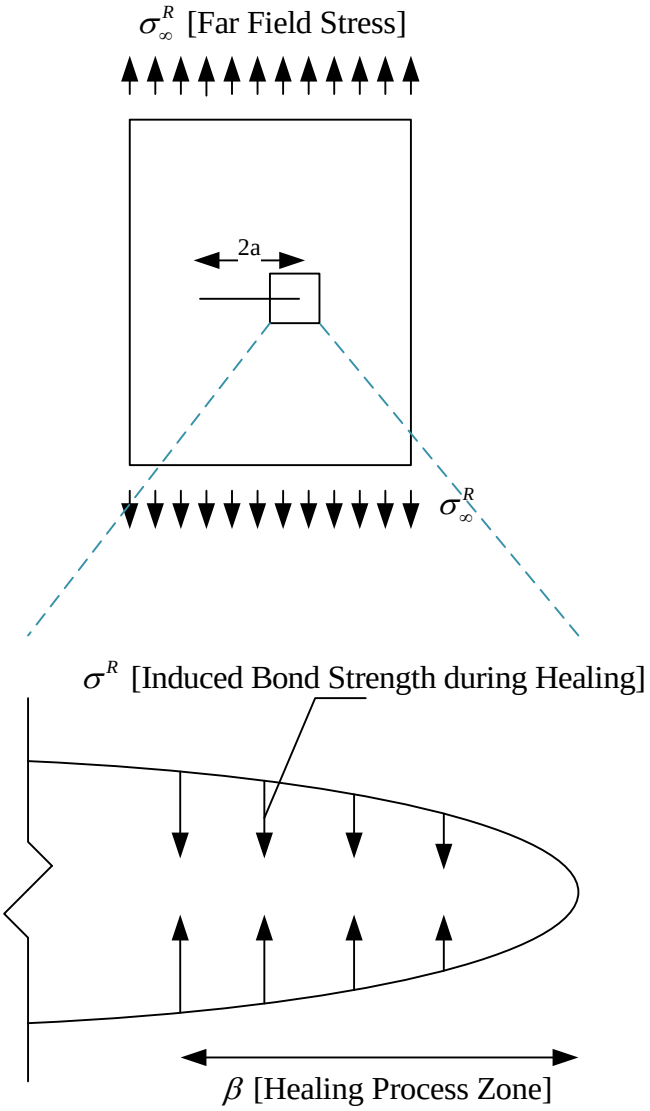

Figure 11: Far field stress applied to the plate containing a centered crack and induced bond strength within the healing process zone.

The superposition principle is also applied to Figure 12(c) in order to calculate its corresponding SIF. Therefore, it is decomposed into the following sub-figures:

1- Traction field is applied in the entire length of the crack as shown in Figure 13 (a).

2-Another force equal but in the opposite direction is applied in the region of $-(a-\beta)$ to $(a-\beta)$, as shown in Figure 13(b).

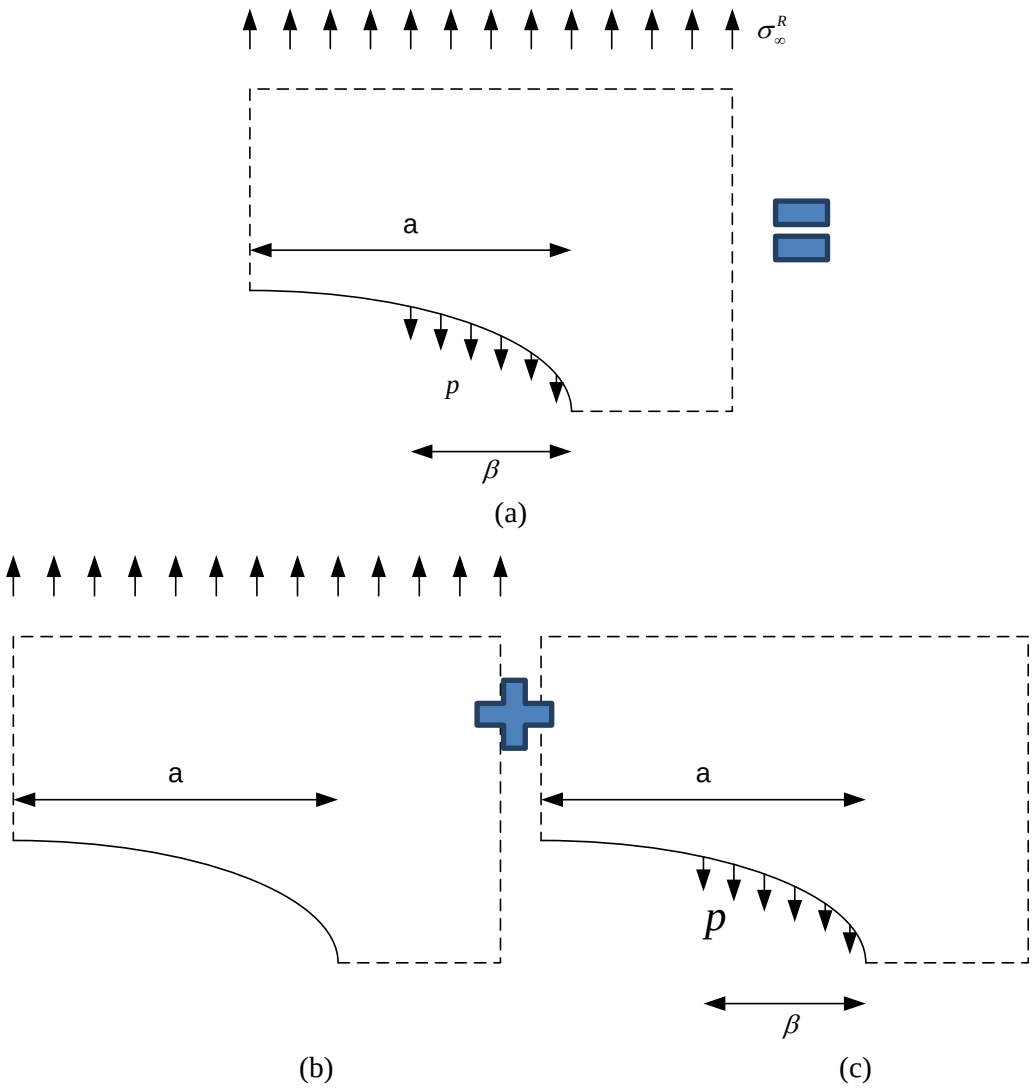

Figure 12: Illustration of superposition principle to solve Mode I crack in the presence of micro-damage healing.

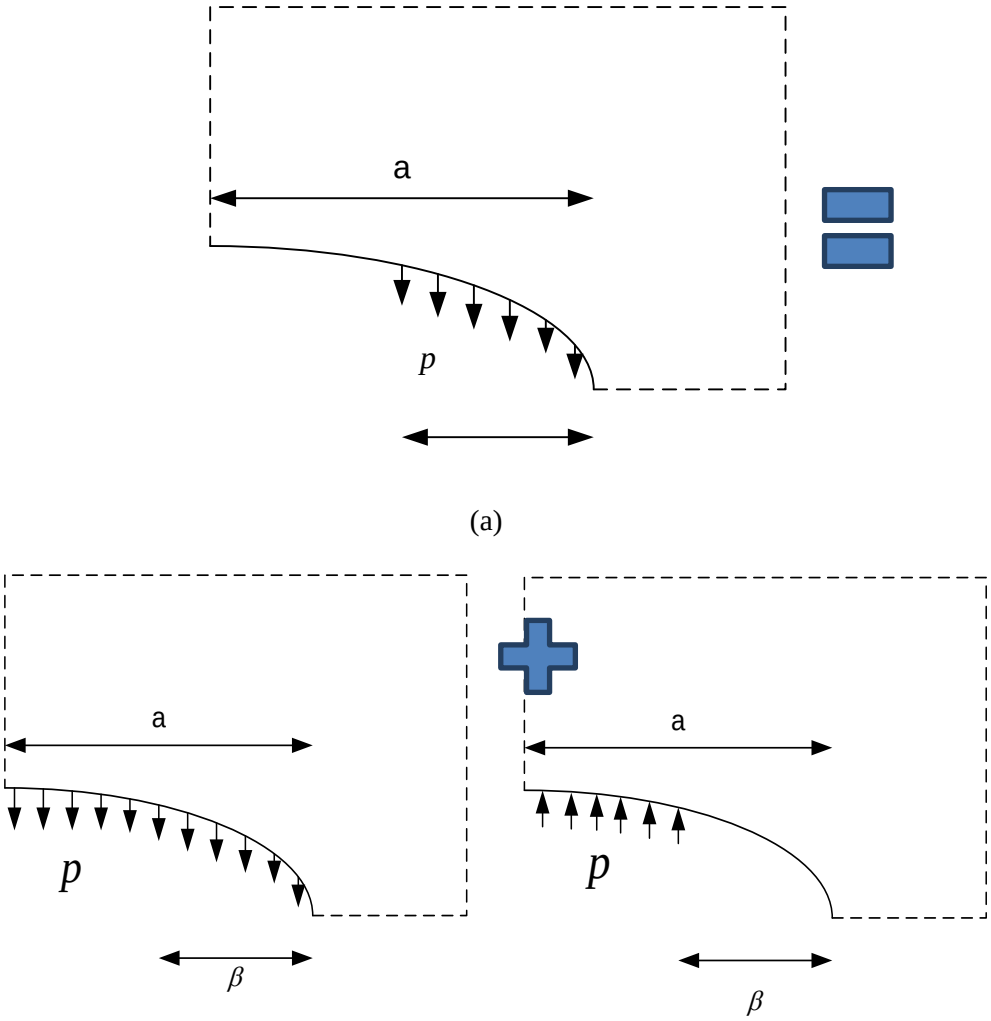

Figure 13: Decomposing stresses shown in Figure 12(c).

The summary of the procedure described above is illustrated in Figure 14.

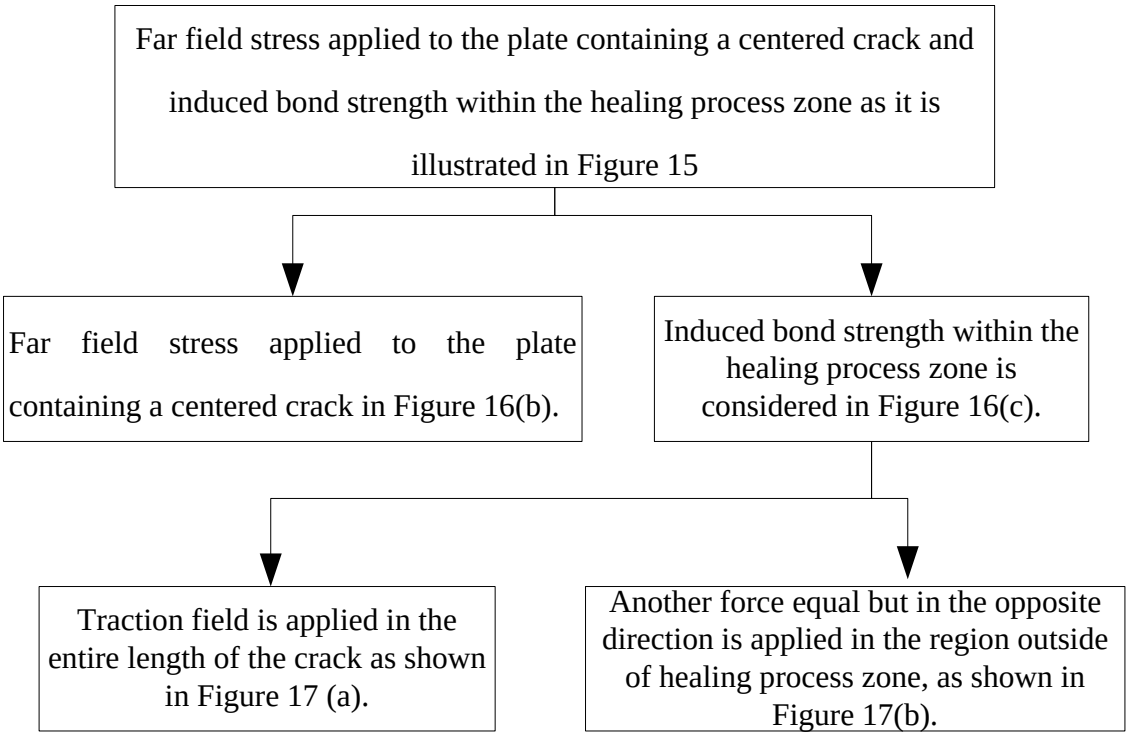

Figure 14: Summary of the procedure to calculate the corresponding SIF.

As mentioned in section 2, stress intensity factor in mode I can be expressed as

$$K_I = \frac{1}{\sqrt{\pi a}} \int_{-a}^{a} g_2(\xi) \sqrt{\frac{a+\xi}{a-\xi}} d\xi \tag{78}$$

where a is the half length of the crack and $g_2(x)$ is the stress function in the vicinity of the crack (Hellan, 1985; Sedov, 1972). This stress function has the value of $-p$ in Figure 13 (a) and p in Figure 13(b). Using the same format as Eq. (77) the SIF of Figure 13(a) is expressed by $K_I = -P\sqrt{\pi a}$. Substituting the value of $g_2(x)$ in Eq. (78), the SIF will be expressed in the following format:

$$K_I = \frac{P}{\sqrt{\pi a}} \int_{-(a-\beta)}^{(a-\beta)} \sqrt{\frac{a+\xi}{a-\xi}} d\xi = \frac{2P\sqrt{a}}{\sqrt{\pi}} \arctan\left(\frac{a-\beta}{\sqrt{\beta}\sqrt{2a-\beta}}\right) \tag{79}$$

Using the superposition principle, the total stress intensity factor (SIF^{Total}) is stated in Eq. (80).

$$K_I^{total} = \sigma_\infty^R \sqrt{\pi a} - P\sqrt{\pi a} + \frac{2P\sqrt{a}}{\sqrt{\pi}} \arctan\left(\frac{a-\beta}{\sqrt{\beta}\sqrt{2a-\beta}}\right) \tag{80}$$

Eq. (80) includes three terms. The first term represents the effect of far field stress on the stress intensity factor. The second term shows the effect of bond strength on reducing the stress intensity factor. Finally, the last term illustrates the effect of the healing process zone characteristics on the stress intensity factor.

To understand how SIF changes with the healing phenomenon, the equation should be written in dimensionless format, such that:

$$NSIF = \frac{K_I^{total}}{\sigma_\infty^R \sqrt{\pi a}} = 1 - \frac{P}{\sigma_\infty^R} + \frac{2}{\pi}\frac{P}{\sigma_\infty^R} \arctan\left(\frac{\frac{a}{\beta}-1}{\sqrt{2\frac{a}{\beta}-1}}\right) \tag{81}$$

The left hand side of Eq. (81) shows the ratio of stress intensity factor with healing properties to the stress intensity factor without considering healing properties. Normalized Stress Intensity Factor (NSIF) ranges from zero to one, such that NSIF=1 indicates no micro-damage healing while NSIF=0 indicates that the micro-damage has been completely healed. This ratio is denoted by the normalized stress intensity factor (NSIF) in the figures.

As the ratio of corresponding healing length to the crack length increases, the normalized SIF decreases. In this case the forces between the upper and lower parts of the crack try to close the opening and therefore the value of SIF decreases. It is also

evident that in order to reach a specific crack opening, the ultimate stress applied at the far field should be greater in order to propagate the crack when the impact of healing or the capability of healing is considered compared to when a material does not possess the capability to heal. On the other hand, as the ratio of bonding strength to the far field stress increases, the normalized SIF decreases. Figure 15 and Figure 16 both show the effect of healing on NSIF.

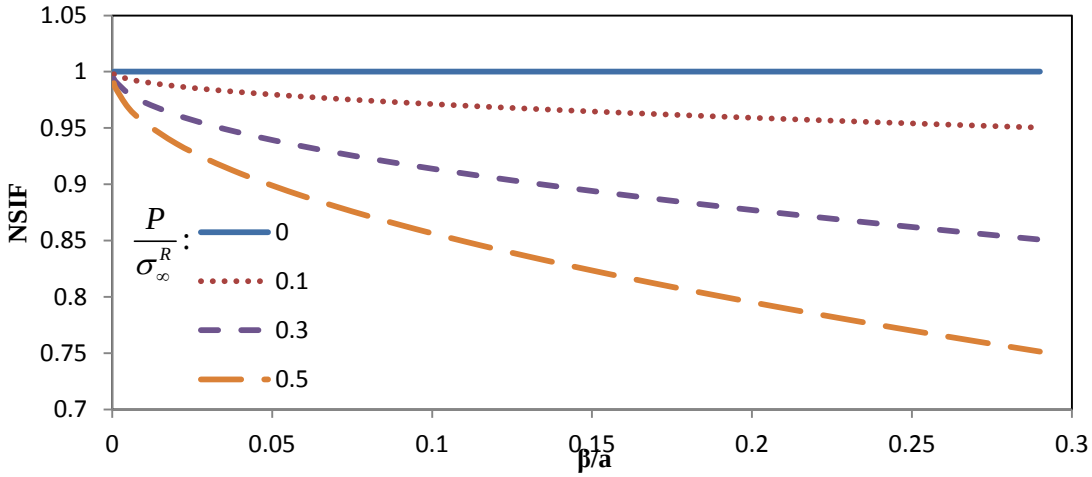

Figure 15: Considering the effect of healing on the normalized stress intensity factor (NSIF). The ratio of $\frac{P}{\sigma_{\infty}^{R}}$ remains constant for each set of data.

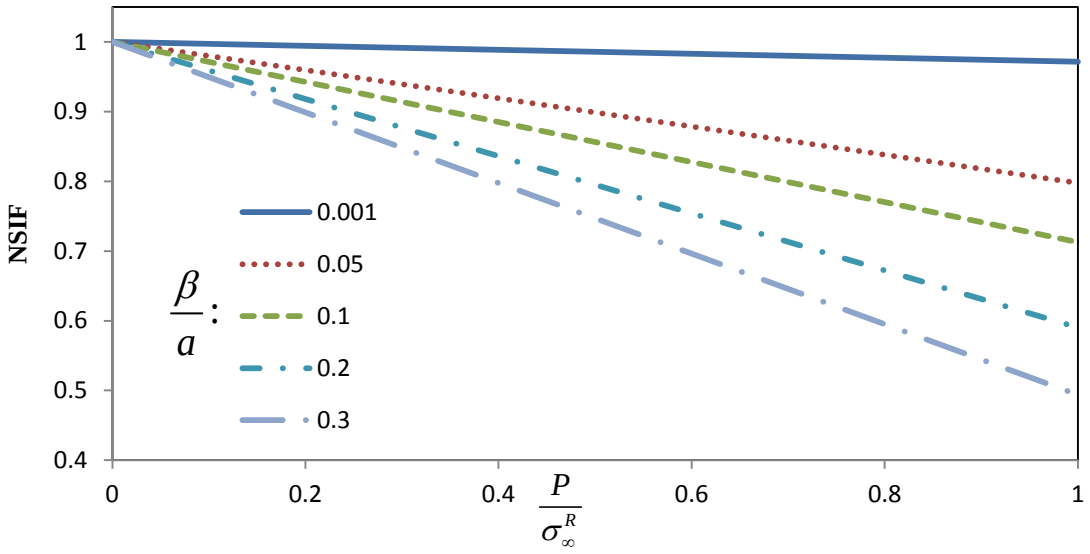

Figure 16: Considering the effect of healing on the normalized stress intensity factor. The ratio of $\frac{\beta}{a}$ remains constant in each set of data.

4.2.2 Elastic media- Considering time-dependent bonding strength

As explained in section 1, the two surfaces came into contact with each other, called wetting in which mechanical property and surface free energy were considered as important factors. Short-term and long-term strength gain, the second stage of healing, was caused by interfacial cohesion and intermolecular diffusion. In the previous step, the bonding strength, p, was assumed to be constant. The next step is to generalize this approach to capture both instantaneous and time-dependent bonding strength as expressed in Eq. (82) to develop an effective model for this phenomenon.

$$\sigma_b(t) = \sigma_0 + (\sigma_b(t_\infty) - \sigma_0)(\frac{t}{t_\infty})^{\frac{1}{4}} \tag{82}$$

where t_r is the rest period, a and b are the healing coefficient and exponent, respectively. Different rest periods result in different values of a and b. Lytton et al. (1993) attained the healing coefficients based on the field data for different climatic zones.

Eq. (2) can be expressed in more detailed format, such that:

$$SF = 1 + (\frac{n_{ri}}{N_0})a(\frac{t_r}{t_0})^h \quad (3)$$

where n_{ri} and N_0 represent the number of rest periods and cycles to fatigue failure, respectively. Moreover, t_0 and t_r express the time between cyclic load and rest period in fatigue test, respectively (Little et al., 2001).

Little et al. (2001) and Lytton et al. (2001) tried to improve the concept of shift factor by implementing the asphalt binders' healing potential, such that:

$$\frac{dh}{dN} = \text{Function}(t_r, h_1, h_2, h_\beta) \quad (4)$$

where h_1 and h_2 are the short-term and long-term healing rate, respectively, and h_β is the maximum healing achieved by the binder. Since $\frac{dh}{dN}$ (rate of healing per load cycle) has the same concept as $\frac{dC}{dN}$ (rate of cracking per load cycle) in fracture mechanics, it can be implemented in fatigue- crack modeling.

1.2 Experimental studies on the significance of micro-damage healing

Developing a model for the healing process is crucial and requires expensive and time-consuming tests. The common laboratory testing practice is to induce resting

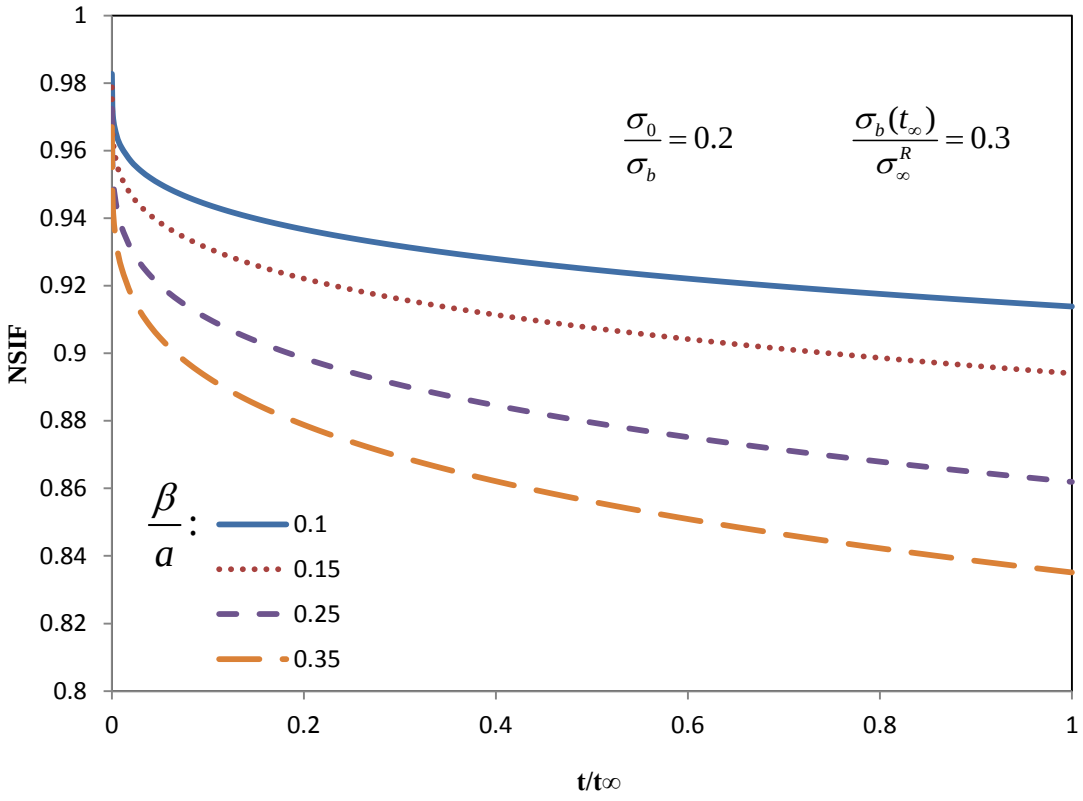

Figure 17: Considering the effect of time on the normalized stress intensity factor (NSIF).

4.3 Effect of micro-damage healing on displacement and stress fields

4.3.1 Elastic media- Neglecting the effect of healing phenomenon

In this section the corresponding calculation of Figure 12(b) is considered. The terminology of stress and displacement near the internal crack is described through a complex-variable technique as mentioned in section 2. The stress and displacement fields are defined by Eqs. (85) and (86).

$$\sigma_{22} = \mathrm{Re}\,\phi' \tag{85}$$

$$u_2 = \frac{1}{2G}\left(\frac{k+1}{2}\mathrm{Im}\,\phi\right) \tag{86}$$

In the first step of computation, the value of ϕ' function must be calculated.

$$\phi_I' = \frac{1}{\pi\sqrt{z^2 - a^2}} \int_{-a}^{a} \frac{\sigma_\infty^R \sqrt{a^2 - \xi^2}}{z - \xi} d\xi \tag{87}$$

With the help of some mathematical manipulation and changing of variables of $\frac{z}{a} = t$ and $\frac{\xi}{a} = x$ the Eq. (87) simplifies to Eq. (88)

$$\phi_I' = \frac{1}{\pi\sqrt{t^2 - 1}} \int_{-1}^{1} \frac{\sigma_\infty^R \sqrt{1 - x^2}}{t - x} dx \tag{88}$$

where t is the arbitrary complex number not lying on the segment [-1, 1] of the real axis. It is noteworthy to talk about the function $\sqrt{t^2 - 1}$ before explaining the procedure to compute Eq. (88). For the large real values of t, this function is real; therefore, the symmetry property is applicable. This means that the value of the function at a complex number t is equal to the complex conjugate value of the function at the conjugate point $\overline{t}$.

$$\begin{gathered} t \in R, t \to \infty \\ f(t) = \overline{f}(\overline{t}) \end{gathered} \tag{89}$$

This function maps purely imaginary values to purely imaginary values, meaning that:

$$t = \alpha i \to \sqrt{t^2 - 1} = \sqrt{-\alpha^2 - 1} = \sqrt{\alpha^2 + 1}(i) \tag{90}$$

One pair of imaginary points with a different sign was assumed. According to the following calculation, two possible answers with opposite signs are found.

$$t=\begin{cases} t_1=\alpha_1 i \rightarrow \sqrt{t_1^{\,2}-1}=\sqrt{(\alpha_1 i)^2-1}=\sqrt{-\alpha_1^{\,2}-1} \\ \rightarrow f(t_1)=\pm\sqrt{\alpha_1^{\,2}+1}(i) \\ t_2=-\alpha_1 i \rightarrow \sqrt{t_2^{\,2}-1}=\sqrt{(-\alpha_1 i)^2-1}=\sqrt{-\alpha_1^{\,2}-1} \\ \rightarrow \overline{f}(t_2)=\pm\sqrt{\alpha_1^{\,2}+1}(i) \end{cases} \qquad (91)$$
$$f(t_1)=\pm\overline{f}(t_2)$$

With the help of a symmetry property ($f(t)=\overline{f}(\overline{t})$), the negative sign in Eq. (91) is shown to be acceptable. Therefore, this function maps each pair of points on the imaginary axis with negative signs to image values on the imaginary axis with negative signs. This property can be extended to the whole domain, and consequently this function is odd.

The residue theorem is applied to solve Eq. (88). The path of this integral consists of a large circle (oriented counter clock-wise) together with an ellipse (oriented clockwise) that surrounds the slit which is clearly seen in Figure 18.

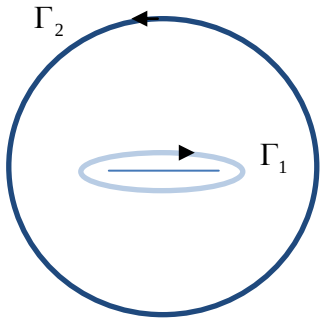

Figure 18: Introducing the contour in the complex plane.

Using the residue theorem, Eq. (92) is derived.

$$\int_{\Gamma_1}\frac{\sqrt{1-x^2}}{t-x}+\int_{\Gamma_2}\frac{\sqrt{1-x^2}}{t-x}=-2\pi\sqrt{t^2-1} \qquad (92)$$

In order to compute the integration over the circular path, the following decomposition is used.

$$\frac{\sqrt{1-x^2}}{t-x} = i + \frac{it}{x-t} + \frac{1}{(t-x)(\sqrt{1-x^2}-ix)}dx \tag{93}$$

$$\int_{\Gamma_1} \frac{\sqrt{1-x^2}}{t-x}dx = -2\pi t + \int_{\Gamma_1} \frac{1}{(t-x)(\sqrt{1-x^2}-ix)}dx \tag{94}$$

The integral in the right hand side of Eq. (94) tends to 0 when the radius expands to a large value. Therefore Eq. (94) simplifies to

$$\int_{\Gamma_1} \frac{\sqrt{1-x^2}}{t-x}dx = -2\pi t \tag{95}$$

Assume that the ellipse (Γ_2) collapses down to a slit. The top part of the ellipse (Γ_1) approaches the slit oriented from left to right, while the bottom part of the ellipse (Γ_1) approaches the slit from right to left. As mentioned before, the value of the integral on the top part is the negative of the value of the integral in the bottom part since the function is odd. As a result Eq. (96) is derived.

$$\int_{\Gamma_1} \frac{\sqrt{1-x^2}}{t-x} = 2\int_{-1}^{1} \frac{\sqrt{1-x^2}}{t-x}dx \tag{96}$$

Using Eq.(94), (95) and (96), the value of equation (88) is computed.

$$-2\pi t + 2\int_{-1}^{1} \frac{\sqrt{1-x^2}}{t-x}dx = -2\pi\sqrt{t^2-1} \rightarrow$$

$$\int_{-1}^{1} \frac{\sqrt{1-x^2}}{t-x}dx = \pi t - \pi\sqrt{t^2-1}$$

$$\phi_I{}' = \frac{1}{\pi\sqrt{t^2-1}}\int_{-1}^{1}\frac{\sigma_\infty^R\sqrt{1-x^2}}{t-x}dx = \frac{\sigma_\infty^R}{\pi\sqrt{t^2-1}}(\pi t - \pi\sqrt{t^2-1}) = \frac{\sigma_\infty^R z}{\sqrt{z^2-a^2}} - \sigma_\infty^R \tag{97}$$

The next step is to integrate the ϕ_I' value determined in Eq. (97).

$$\phi_I = \sigma_\infty^R\sqrt{z^2-a^2} - \sigma_\infty^R z + const. \tag{98}$$

As mentioned before, the stress near the crack tip is computed by means of Eq. (85). The crack is oriented in the x direction; therefore the variable z is converted to variable x.

$$\sigma_{22} = \mathrm{Re}\,\phi' = \mathrm{Re}\left(\frac{\sigma_\infty^R x}{\sqrt{x^2-a^2}} - \sigma_\infty^R + \sigma_\infty^R\right) \tag{99}$$

As a result, σ_{22} is equal to $\frac{\sigma_\infty^R x}{\sqrt{x^2-a^2}}$ for $|x| \geq a$ and 0 for $|x| \prec a$. Also the displacement field can be calculated with the help of Eqs. (86) and (97).

$$u_2 = \frac{1}{2G}\left(\frac{k+1}{2}\mathrm{Im}\,\phi\right) = \frac{1}{2G}\frac{k+1}{2}\mathrm{Im}(\sigma_\infty^R\sqrt{z^2-a^2} - \sigma_\infty^R z + const.)$$

$$u_2 = \pm\frac{k+1}{4G}\sigma_\infty^R\sqrt{a^2-x^2} \tag{100}$$

4.3.2 Elastic media- Considering constant bond strength p

This case is fully explained in Figure 13. The function of ϕ_I' must be defined for both cases described in Figure 13 (a) and (b). The calculation of Figure 13(a) is similar to what was previously explained but with the difference in the value of the stress. Instead of having σ_∞^R, the stress $-p$ is replaced. ϕ_I' value for the case described in Figure 13(a) is denoted by $\phi_I'(1)$ and explained in Eq. (101).

$$\phi_I'(1) = \frac{1}{\pi\sqrt{t^2-1}} \int_{-1}^{1} \frac{-p\sqrt{1-x^2}}{t-x} dx = \frac{-pz}{\sqrt{z^2-a^2}} + p \tag{101}$$

The corresponding stress and displacement fields with analogy to the previous part are written in Eq. (102) and (103).

$$u_2 = -\frac{k+1}{4G} p\sqrt{a^2-x^2} \tag{102}$$

$$\sigma_{22} = \mathrm{Re}\left(\frac{-px}{\sqrt{x^2-a^2}}\right) \tag{103}$$

As described in Figure 13(b), the bonding strength is defined over a part of the region; therefore, the equation ϕ_I' is expressed in the following format denoted by $\phi_I'(2)$.

$$\begin{aligned} \phi_I'(2) &= \frac{1}{\pi\sqrt{z^2-a^2}} \int_{-(a-\beta)}^{(a-\beta)} \frac{p\sqrt{a^2-\xi^2}}{z-\xi} d\xi \\ \phi_I'(2) &= \frac{2pz}{\pi\sqrt{z^2-a^2}} \arcsin\left(\frac{a-\beta}{a}\right) - \frac{2p}{\pi} \arctan\left(\frac{(a-\beta)\sqrt{z^2-a^2}}{z\sqrt{2a\beta-\beta^2}}\right) \end{aligned} \tag{104}$$

Before going through the rest of the calculation, further explanation seems essential of the procedure necessary to derive Eq. (104). Changing of variables and

doing some mathematical manipulations, the first row of Eq. (104) changes into Eq. (105)

$$\frac{p}{\pi\sqrt{z^2-a^2}}\int_{-(a-\beta)}^{(a-\beta)}\frac{\sqrt{a^2-\xi^2}}{z-\xi}d\xi=\frac{p}{\pi\sqrt{z'^2-1}}\int_{-b'}^{b'}\frac{\sqrt{1-x^2}}{z'-x}dx \qquad (105)$$

where $\frac{\xi}{a}$ changes into x, $\frac{z}{a}$ changes into z', and finally, b' represents the value of $\frac{\alpha-\beta}{\alpha}$. The new proposition is to prove if $0<b'<1$, and z' is a complex number not lying in the segment $[-b',b']$ of the real axis, then

$$\frac{p}{\pi\sqrt{z'^2-1}}\int_{-b'}^{b'}\frac{\sqrt{1-x^2}}{z'-x}dx=\frac{2pz}{\pi\sqrt{z^2-a^2}}\arcsin(\frac{a-\beta}{a})-\frac{2p}{\pi}\arctan(\frac{(a-\beta)\sqrt{z^2-a^2}}{z\sqrt{2a\beta-\beta^2}})$$

(106)

Since z' is excluded from the integration path, the left hand side of Eq. (106) encounters no singularity. Therefore, the integral represents an analytic function of z'. Since b' has a positive value less than one, function $\arcsin b'$ is well-defined. The tangent function can be written in terms of the complex exponential function, as shown in Eq. (107).

$$\arctan w=\frac{1}{2i}\ln\frac{1+iw}{1-iw} \qquad (107)$$

The hypothesis that z is outside the integral path guarantees that the arctan in Eq. (106) is well-defined. Therefore, both sides of Eq. (106) are analytic functions of z.

In order to solve Eq. (106) , the variable x is replaced by $\frac{2u}{1+u^2}$. Therefore the following equation can be expressed.

$$\sqrt{1-x^2}=\frac{1-u^2}{1+u^2};\quad dx=\frac{2(1-x^2)}{(1+x^2)^2} \tag{108}$$

Eq. (106) changes into:

$$\frac{p}{\pi\sqrt{z'^2-1}}\int_{-b'}^{b'}\frac{\sqrt{1-x^2}}{z'-x}dx=\frac{p}{\pi\sqrt{z'^2-1}}(2\int_{-c'}^{c'}\frac{(1-u^2)^2}{(1+u^2)^2}\frac{1}{(1+u^2)z'-2u}du) \tag{109}$$

where $c'=(1-\sqrt{1-b'^2})/b'$. The method of partial fractions is applied to derive Eq. (110) .

$$\frac{(1-u^2)^2}{(1+u^2)^2}\frac{1}{(1+u^2)z'-2u}=\frac{-(z'^2-1)}{z'u^2+z-2u}+\frac{z}{u^2+1}+\frac{2u}{(u^2+1)^2} \tag{110}$$

The third term integrates to 0 by symmetry. Moreover, the second term can be written in terms of $\arctan c$. Therefore Eq. (110) reduces to:

$$-2(z'^2-1)\int_{-c'}^{c'}\frac{1}{z'u^2+z-2u}du+4z\arctan(c') \tag{111}$$

Since $\frac{1}{z'u^2+z-2u}=\frac{z'}{(z'u-1)^2+z^2-1}=\frac{1}{\sqrt{z'^2-1}}\cdot\frac{\frac{z'}{\sqrt{z'^2-1}}}{(\frac{z'u-1}{\sqrt{z'^2-1}})^2+1}$, it follows that $\int\frac{1}{z'u^2+z-2u}du=\frac{1}{\sqrt{z'^2-1}}\arctan\left(\frac{z'u-1}{z'^2-1}\right)$.

Using a mathematical identity ($\arctan(A)+\arctan(B)=\arctan(\frac{A+B}{1-AB})$) and the above calculations, Eq. (111) simplifies to:

$$-2(z'^2-1)\arctan(\frac{2c'\sqrt{z'^2-1}}{(1-c'^2)z'})+4z\arctan(c') \tag{112}$$

Identity shows that $2\arctan(c') = \arctan(\frac{2c'}{1-c'^2})$, so the result becomes $-2\sqrt{z'^2-1}\arctan(\frac{2c'\sqrt{z'^2-1}}{(1-c'^2)z'}) + 2\arctan(\frac{2c'}{1-c'^2})$. An algebraic calculation proves that $\frac{2c'}{1-c'^2} = \frac{b'}{\sqrt{1-b'^2}}$. Therefore, Eq. (104) is derived.

Denoting $\frac{a-\beta}{a} = c$ makes our calculation much simpler to represent.

$$\phi_I'(2) = \frac{2pz}{\pi\sqrt{z^2-a^2}}\arcsin(c) - \frac{2p}{\pi}\arctan(\frac{c\sqrt{z^2-a^2}}{z\sqrt{1-c^2}}) \tag{113}$$

The value of $\phi_I(2)$ is calculated using integration.

$$\phi_I(2) = \frac{2p}{\pi}\arcsin(\frac{a-\beta}{a})\sqrt{z^2-a^2} - \frac{2p}{\pi}\int\arctan(\frac{(a-\beta)\sqrt{z^2-a^2}}{z\sqrt{2a\beta-\beta^2}})dz$$

$$\phi_I(2) = \frac{2p}{\pi}\arcsin(c)\sqrt{z^2-a^2} - \frac{2p}{\pi}(z\times\arctan(\frac{c}{\sqrt{1-c^2}}\frac{\sqrt{z^2-a^2}}{z}) \tag{114}$$

$$-ac\times\arctan(\frac{1}{\sqrt{1-c^2}}\frac{\sqrt{z^2-a^2}}{a}))$$

The displacement field is evaluated by the use of Eq. (86). Therefore, the imaginary part of function $\phi_I(2)$ is needed.

$$u_2(2) = \frac{k+1}{4G}\frac{2p}{\pi}\arcsin(c)\sqrt{a^2-x^2} \tag{115}$$

The stress is defined by using Eq. (31) and (104).

$$\sigma_{22}(2) = \mathrm{Re}\,\phi' = \mathrm{Re}(\frac{2px}{\pi\sqrt{x^2-a^2}}\arcsin(c) - \frac{2p}{\pi}\arctan(\frac{c\sqrt{x^2-a^2}}{x\sqrt{1-c^2}})) \tag{116}$$

Using superposition method, the displacement and stress fields are described in Eq. (117) and (119), respectively.

$$u_2 = \frac{k+1}{4G}\sigma_\infty^R\sqrt{a^2-x^2} - \frac{k+1}{4G}p\sqrt{a^2-x^2} + \frac{k+1}{4G}\frac{2p}{\pi}(\arcsin(c)\sqrt{a^2-x^2} - x\times\arctan(\frac{c}{\sqrt{1-c^2}}\frac{\sqrt{a^2-x^2}}{x}) + ac\times\arctan(\frac{1}{\sqrt{1-c^2}}\frac{\sqrt{a^2-x^2}}{a})) \quad (117)$$

In order to have figures of the displacement field, its equation must be presented in the following dimensionless format.

$$\frac{u_2}{\frac{k+1}{4G}a\sigma_\infty^R} = \sqrt{1-(\frac{x}{a})^2} - \frac{p}{\sigma_\infty^R}\sqrt{1-(\frac{x}{a})^2} + \frac{2}{\pi}\frac{p}{\sigma_\infty^R}(\arcsin(c)\sqrt{1-(\frac{x}{a})^2} - \frac{x}{a}\times\arctan(\frac{c}{\sqrt{1-c^2}}\frac{\sqrt{1-(\frac{x}{a})^2}}{\frac{x}{a}}) + c\times\arctan(\frac{1}{\sqrt{1-c^2}}\sqrt{1-(\frac{x}{a})^2})) \quad (118)$$

Figure shows the displacement field near the crack tip. Term $\frac{u_2}{\frac{k+1}{4G}a\sigma_\infty^R}$ on the left-hand side of Eq. (118) is called the normalized displacement (NU). At the crack point the displacement is zero, but moving away from the crack tip the displacement is shown to increase. The ratio of $\frac{p}{\sigma_\infty^R}$ varies while the value of c remains constant in each figure. For a constant value of c, as the value of $\frac{p}{\sigma_\infty^R}$ increases the normalized

displacement decreases. This clearly shows that the healing phenomenon tends to reduce the distance between the upper and lower part of the micro-crack. Also, it can be seen that the normalized displacement in Figure (a) is less than the normalized displacement in Figure(b) for the region $0.95 < \frac{x}{a} < 1$ due to greater bonding zone.

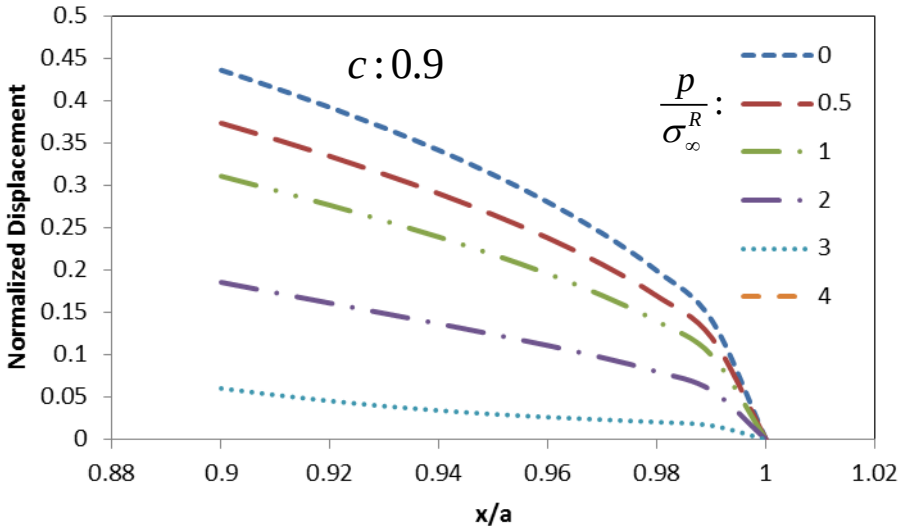

(a)

Figure 19: Displacement field near the crack tip under constant value of c.

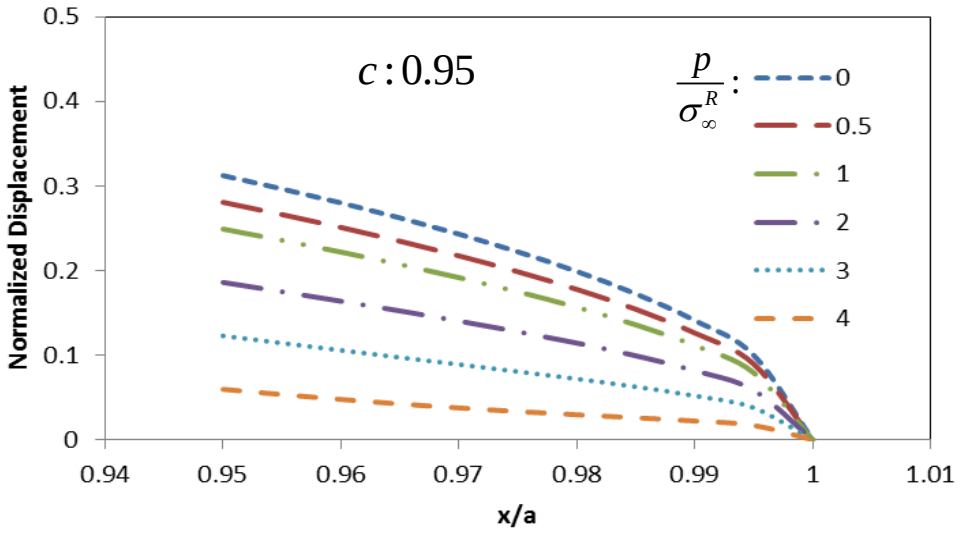

(b)

Figure 19: Continued.

Figure 20 shows the displacement field near the crack tip under constant value of $\frac{p}{\sigma_{\infty}^{R}}$. The ratio of c varies while the value of $\frac{p}{\sigma_{\infty}^{R}}$ remains constant in each figure. In other words, it demonstrates the effect of different healing process zone in displacement fields. For a constant value of $\frac{p}{\sigma_{\infty}^{R}}$, as the value of c decreases, the normalized displacement decreases. This clearly shows that the healing phenomenon tends to reduce the distance between the upper and lower parts of the micro-crack. Also, it can be seen that the normalized displacement in Figure 20(b) is less than the normalized displacement in Figure 20(a) for the corresponding bonding region due to greater bonding strength. The effect of different healing process zone on stress field is discussed afterwards.

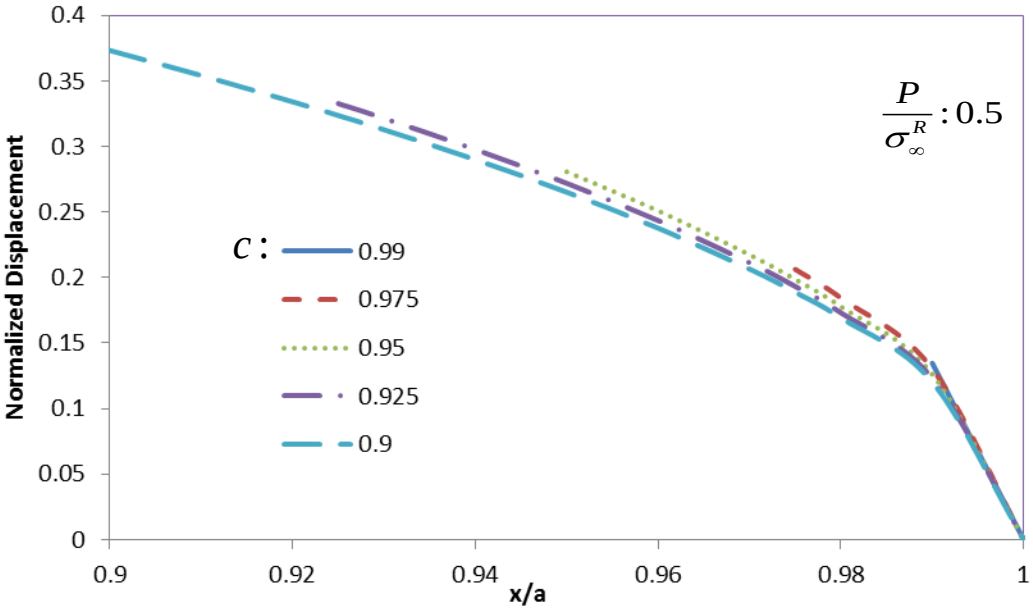

(a)

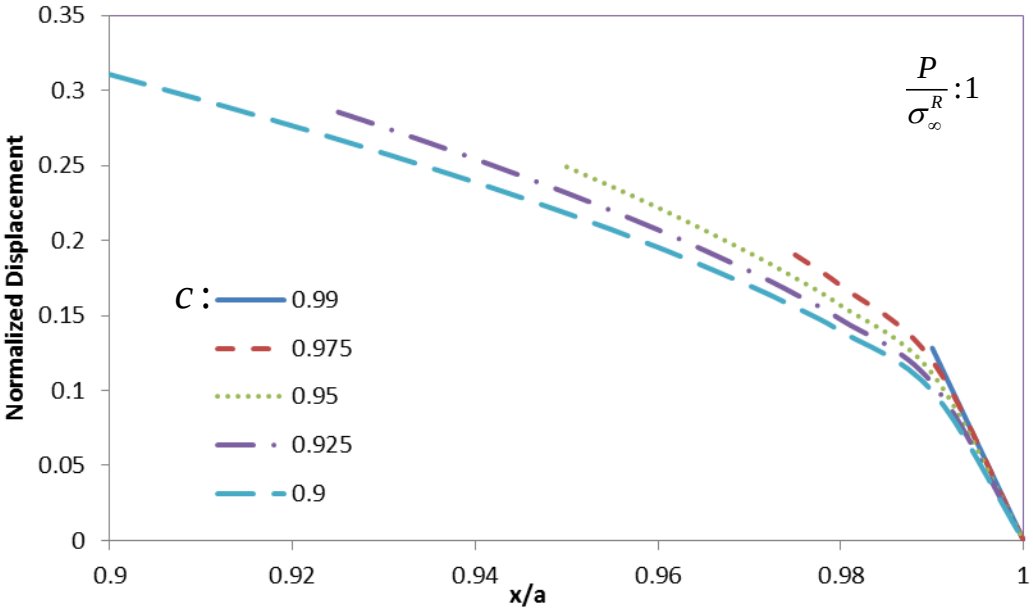

(b)

Figure 20: Displacement field near the crack tip under constant value of $\frac{p}{\sigma_\infty^R}$.

$$\sigma_{22} = \mathrm{Re}\left(\frac{\sigma_\infty^R x}{\sqrt{x^2-a^2}}\right) + \mathrm{Re}\left(\frac{-px}{\sqrt{x^2-a^2}}\right) + \mathrm{Re}\left(\frac{2px}{\pi\sqrt{x^2-a^2}}\arcsin\left(\frac{a-\beta}{a}\right) - \frac{2p}{\pi}\arctan\left(\frac{(a-\beta)\sqrt{x^2-a^2}}{x\sqrt{2a\beta-\beta^2}}\right)\right)$$

$$\frac{\sigma_{22}}{\sigma_\infty^R} = \mathrm{Re}\left(\frac{1}{\sqrt{1-\left(\frac{a}{x}\right)^2}}\right) + \mathrm{Re}\left(\frac{-\frac{p}{\sigma_\infty^R}}{\sqrt{1-\left(\frac{a}{x}\right)^2}}\right) + \mathrm{Re}\left(\frac{2}{\pi\sqrt{1-\left(\frac{a}{x}\right)^2}}\frac{p}{\sigma_\infty^R}\arcsin\left(1-\frac{\beta}{a}\right) - \frac{2}{\pi}\frac{p}{\sigma_\infty^R}\arctan\left(\frac{\left(1-\frac{\beta}{a}\right)\sqrt{1-\left(\frac{a}{x}\right)^2}}{\sqrt{2\frac{\beta}{a}-\left(\frac{\beta}{a}\right)^2}}\right)\right) \quad (119)$$

Eq. (119) has the value of

$$\frac{\sigma_\infty^R x}{\sqrt{x^2-a^2}} - \frac{px}{\sqrt{x^2-a^2}} + \frac{2px}{\pi\sqrt{x^2-a^2}}\arcsin\left(\frac{a-\beta}{a}\right) - \frac{2p}{\pi}\arctan\left(\frac{(a-\beta)\sqrt{x^2-a^2}}{x\sqrt{2a\beta-\beta^2}}\right)$$

for $|x| \geq a$ and 0 for $|x| \prec a$.

As the value of $\frac{a}{x}$ goes to infinity, the ratio of $\frac{\sigma_{22}}{\sigma_\infty^R}$ reaches the value of $1-\frac{p}{\sigma_\infty^R}$, which can be clearly seen in both Figure 21 and Figure 22. Figure 21 shows the stress field near the crack tip under constant value of $\frac{p}{\sigma_\infty^R}$. The term $\frac{\sigma_{22}}{\sigma_\infty^R}$ in the left-hand side of Eq. (118) is called the normalized stress (NS). At the crack point, the stress goes to infinity as it was fully explained in SIF section, but moving away from the crack tip, the stress decreases. The ratio of $\frac{\beta}{a}$ varies in each figure while the value of $\frac{p}{\sigma_\infty^R}$ remains constant. For a constant value of $\frac{p}{\sigma_\infty^R}$, as the value of $\frac{\beta}{a}$ increases, the normalized stress

decreases. Also it can be seen that normalized stress in Figure 21(b) is less than the normalized stress in Figure 21(a) due to greater bonding strength.

Figure 22 shows the stress field near the crack tip under the constant value of $\frac{\beta}{a}$. The ratio of $\frac{p}{\sigma_\infty^R}$ varies in each figure while the value of $\frac{\beta}{a}$ remains the same. For a constant value of $\frac{\beta}{a}$, as the value of $\frac{P}{\sigma_\infty^R}$ increases, the normalized stress decreases. Also, it can be seen that normalized stress in Figure 22(b) is less than the normalized stress in Figure 22(a) due to greater bonding zone. As mentioned before, the ratio of $\frac{\sigma_{22}}{\sigma_\infty^R}$ reaches the value of $1-\frac{p}{\sigma_\infty^R}$ when the value of $\frac{a}{x}$ goes to 0. Also, it must be mentioned that when $\frac{p}{\sigma_\infty^R}$ is greater than 1, the stress could become compressive since it represents the case when crack faces are under compressive stress states. Therefore, the compressive normalized stress is not plotted in this case.

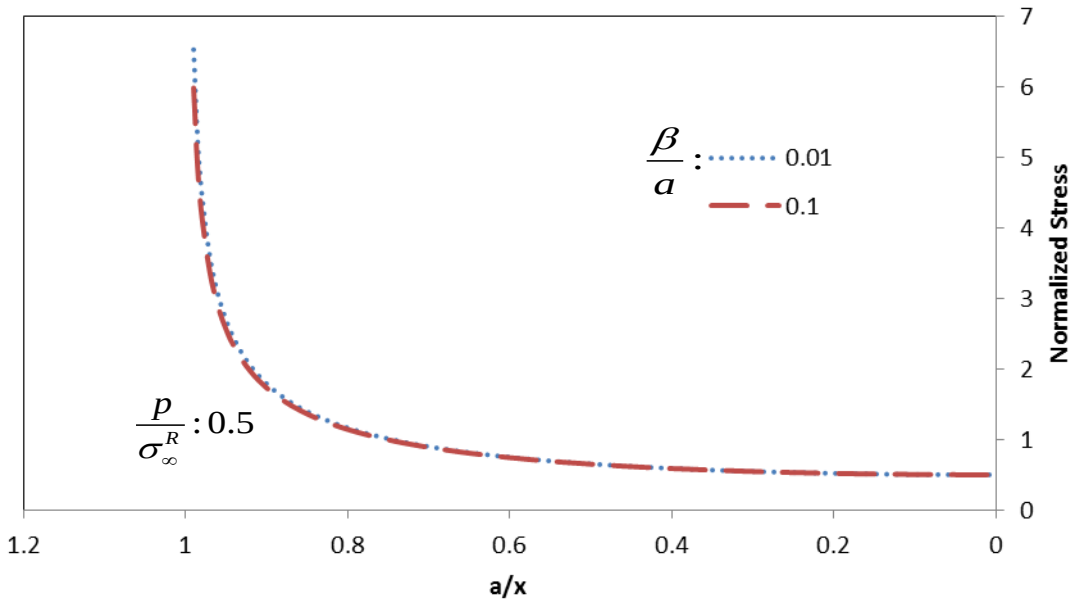

(a)

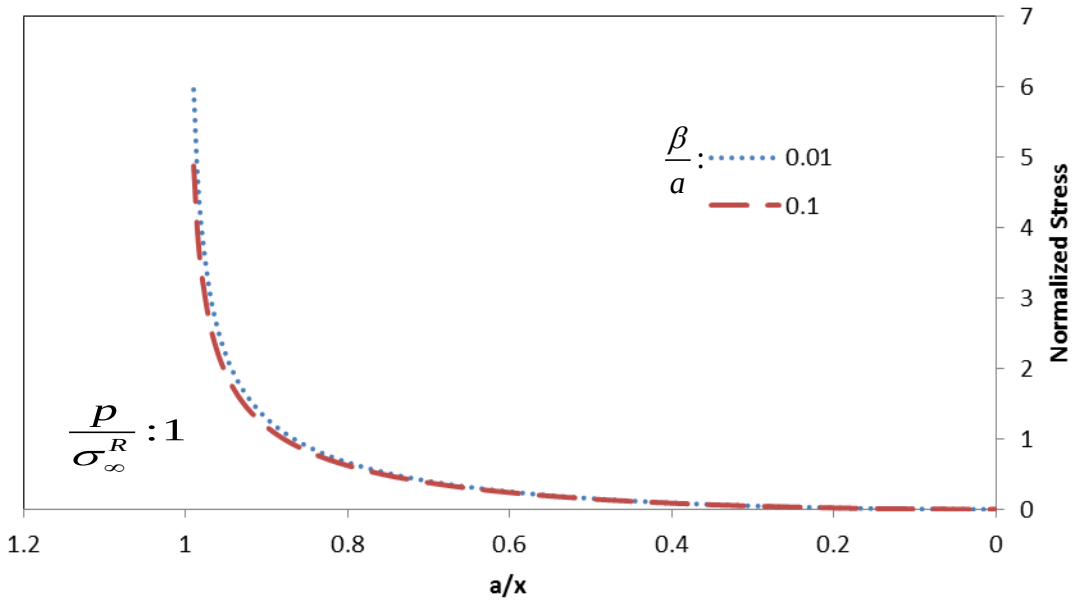

(b)

Figure 21: Stress field near the crack tip under constant value of $\frac{p}{\sigma_\infty^R}$.

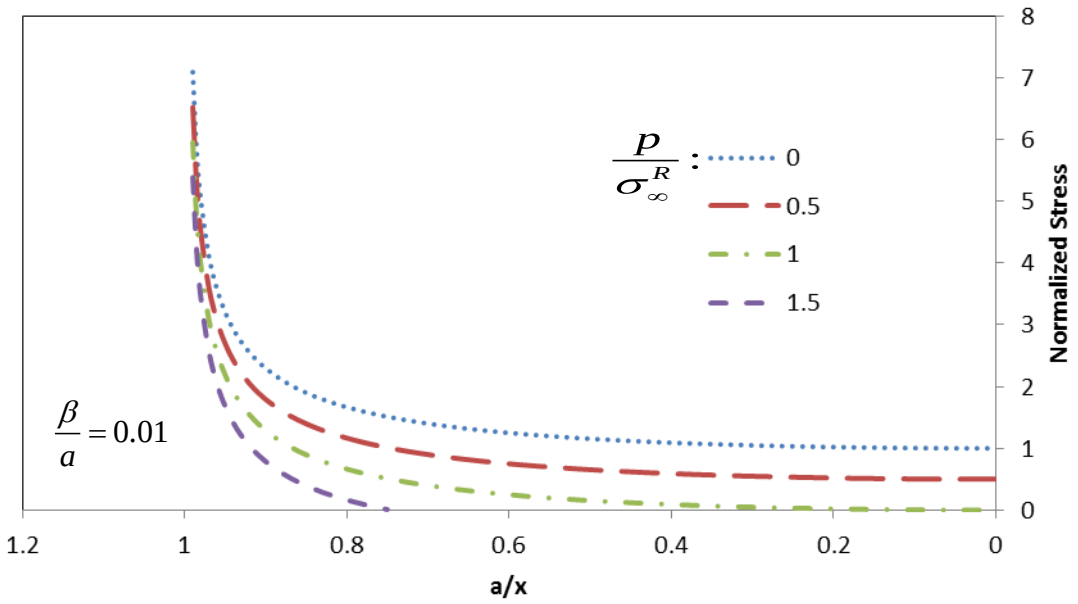

(a)

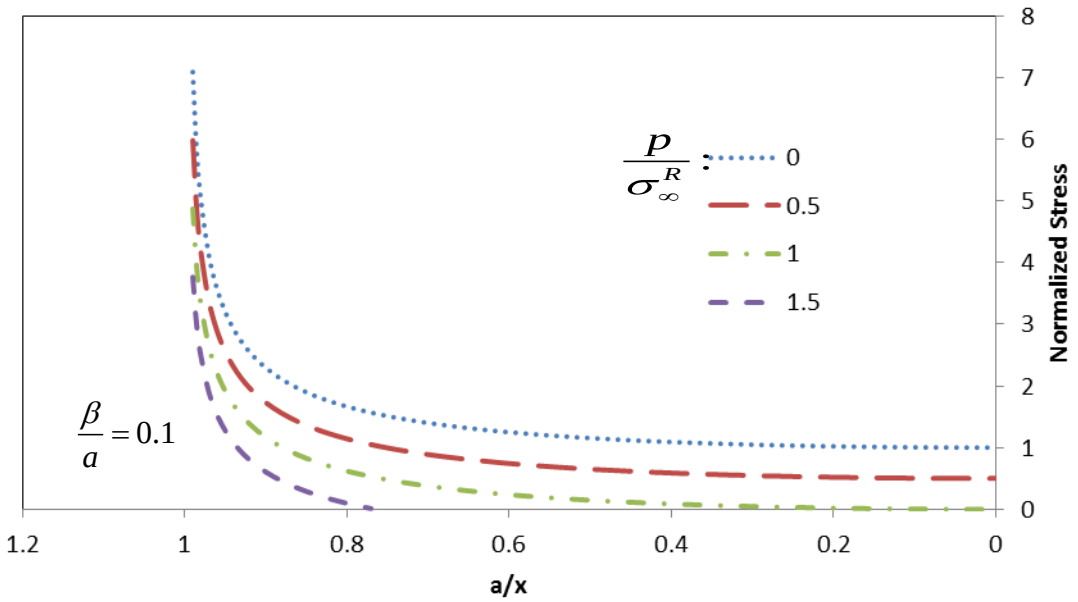

(b)

Figure 22: Showing stress field near the crack tip under constant value of $\frac{\beta}{a}$.

4.3.3 Elastic media- Loading-unloading scenario

In this part the far field stress does not remain constant any more. The effect of triangular loading and unloading on displacement and stress fields is evaluated. The period of loading and unloading cycles are assumed to be equal to T. The far field stress is written in terms of σ_{∞}^{R} using $\frac{\sigma_{\infty}^{R}(t)}{\sigma_{\infty}^{R}} = F$, where F is defined as stress factor and can be expressed by a value in range $0 \le F \le 1$. The far field stress loading and unloading cycles is shown in Figure 23.

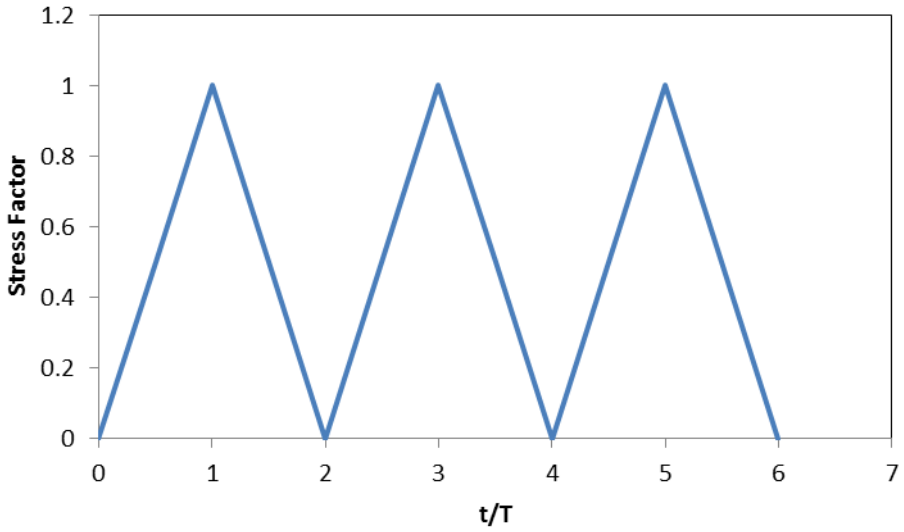

Figure 23: Far field stress loading and unloading cycles.

Displacement and stress field are expressed in Eqs. (120) and (121).

$$\frac{u_2}{\frac{k+1}{4G}a\sigma_\infty^R} = F\sqrt{1-(\frac{x}{a})^2} - \frac{p}{\sigma_\infty^R}\sqrt{1-(\frac{x}{a})^2} +$$

$$\frac{2}{\pi}\frac{p}{\sigma_\infty^R}(\arcsin(c)\sqrt{1-(\frac{x}{a})^2} - \frac{x}{a}\times\arctan(\frac{c}{\sqrt{1-c^2}}\frac{\sqrt{1-(\frac{x}{a})^2}}{\frac{x}{a}}) + \tag{120}$$

$$c\times\arctan(\frac{1}{\sqrt{1-c^2}}\sqrt{1-(\frac{x}{a})^2}))$$

$$\frac{\sigma_{22}}{\sigma_\infty^R(t)} = \frac{x}{\sqrt{x^2-a^2}} - \frac{p}{\sigma_\infty^R(t)}\frac{x}{\sqrt{x^2-a^2}} + \frac{2x}{\pi\sqrt{x^2-a^2}}\frac{p}{\sigma_\infty^R(t)}\arcsin(\frac{a-\beta}{a}) -$$

$$\frac{2}{\pi}\frac{p}{\sigma_\infty^R(t)}\arctan(\frac{(a-\beta)\sqrt{x^2-a^2}}{x\sqrt{2a\beta-\beta^2}})$$

$$\frac{\sigma_{22}}{\sigma_\infty^R} = F\frac{1}{\sqrt{1-(\frac{a}{x})^2}} - \frac{p}{\sigma_\infty^R}\frac{1}{\sqrt{1-(\frac{a}{x})^2}} + \frac{2}{\pi}\frac{p}{\sigma_\infty^R}\frac{1}{\sqrt{1-(\frac{a}{x})^2}}\arcsin(c) - \tag{121}$$

$$\frac{2}{\pi}\frac{p}{\sigma_\infty^R}\arctan(\frac{c\sqrt{1-(\frac{a}{x})^2}}{\sqrt{1-c^2}})$$

As the value of F increases, the loading scenario is considered. As a result, the normalized displacement also increases, which can be clearly seen in the Figure 24. Comparing the results of Figure 24(a) and (b), for the constant value of c, as the ratio of $\frac{p}{\sigma_\infty^R}$ increases, the normalized displacement decreases.

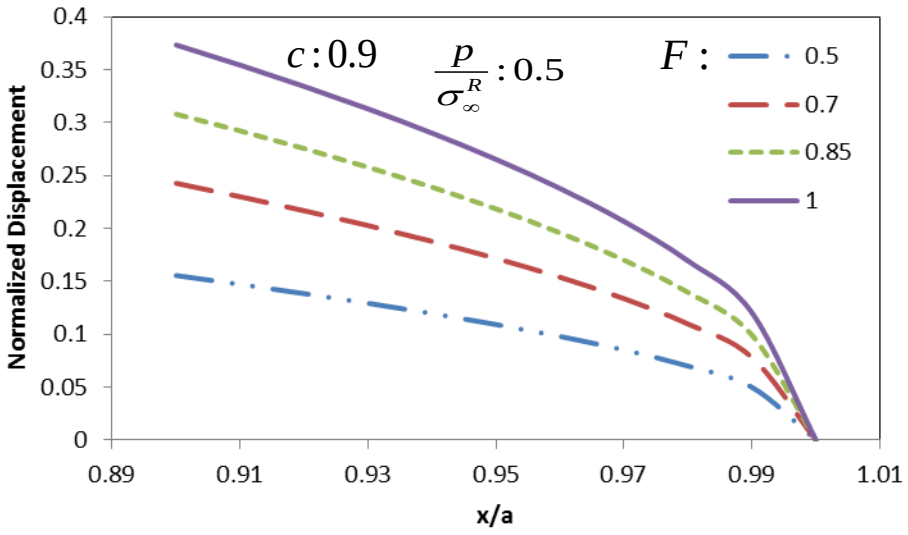

(a)

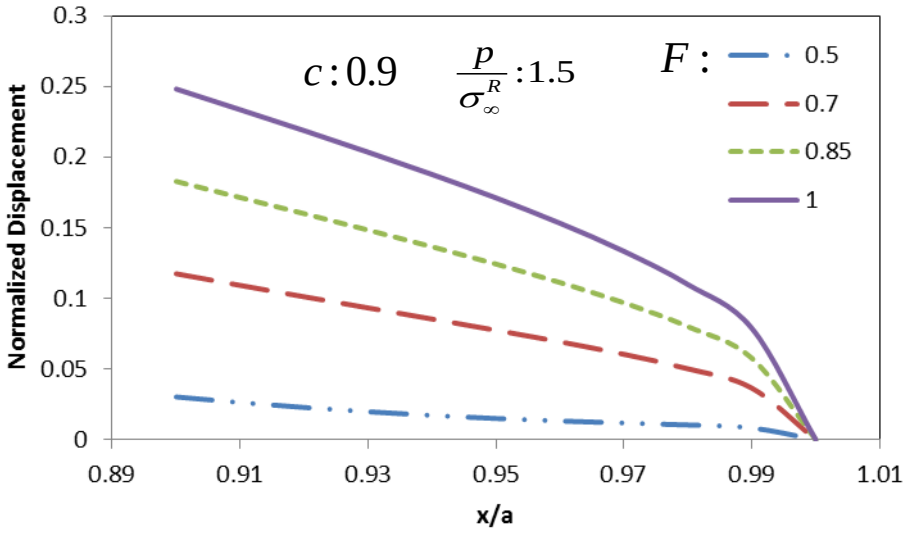

(b)

Figure 24: Normalized displacement under loading and unloading cycle.

Figure 25 shows the displacement field near the crack tip under loading and unloading cycles. The ratio of $\frac{p}{\sigma_{\infty}^{R}}$ is constant while the value of c varies in each figure. In other words, the effect of different healing process zone is considered. For a constant value of $\frac{p}{\sigma_{\infty}^{R}}$, as the value of c increases, the normalized displacement decreases. It clearly shows that the healing phenomenon tends to reduce the distance between the upper and lower part of the micro-crack. Also it can be seen that normalized displacement in Figure 25(a) is less than the normalized displacement in Figure 25(b) for the region $0.95 < \frac{x}{a} < 1$ due to a greater bonding zone.

The effect of different values of F, c and $\frac{p}{\sigma_{\infty}^{R}}$ on stress field is evaluated afterwards. In Figure 26, the value of c remains constant and the effect of change in the value of $\frac{p}{\sigma_{\infty}^{R}}$ is considered. Comparing Figure 26(a) and Figure 26(b) shows that an increase in $\frac{p}{\sigma_{\infty}^{R}}$ results in a decrease in the stress field. This phenomenon is compatible with the fact that healing tries to close the micro cracks; therefore, it reduces the stress field. Also it is evident that an increase in the value F leads to an increase in the value of stress field.

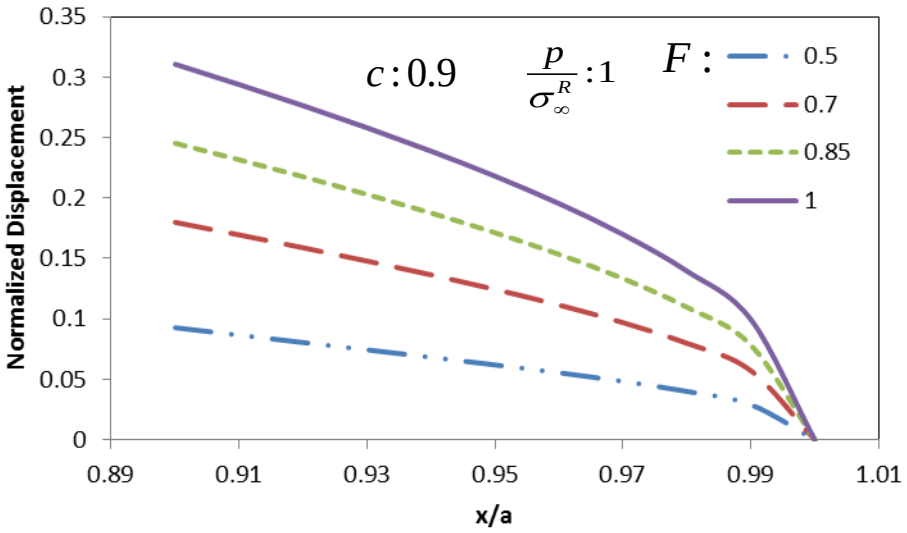

(a)

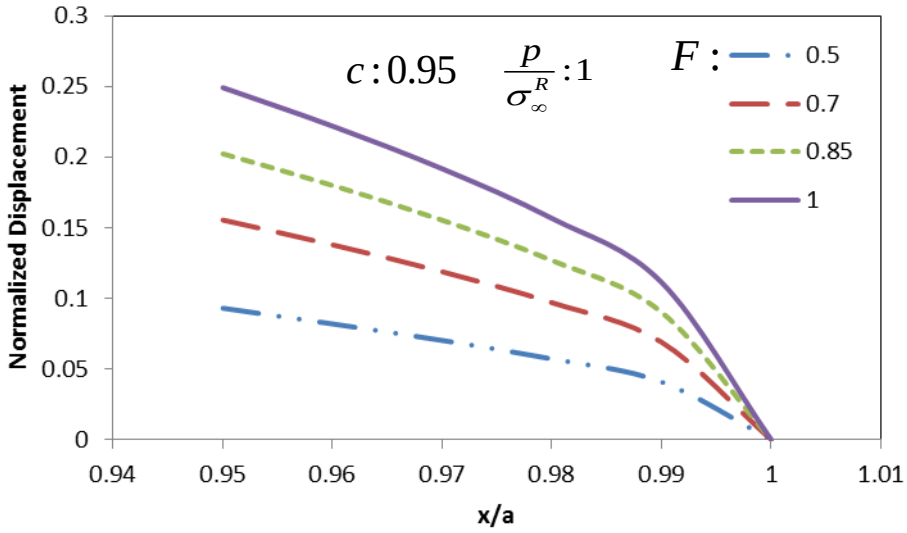

(b)

Figure 25: Normalized displacement under loading and unloading cycle

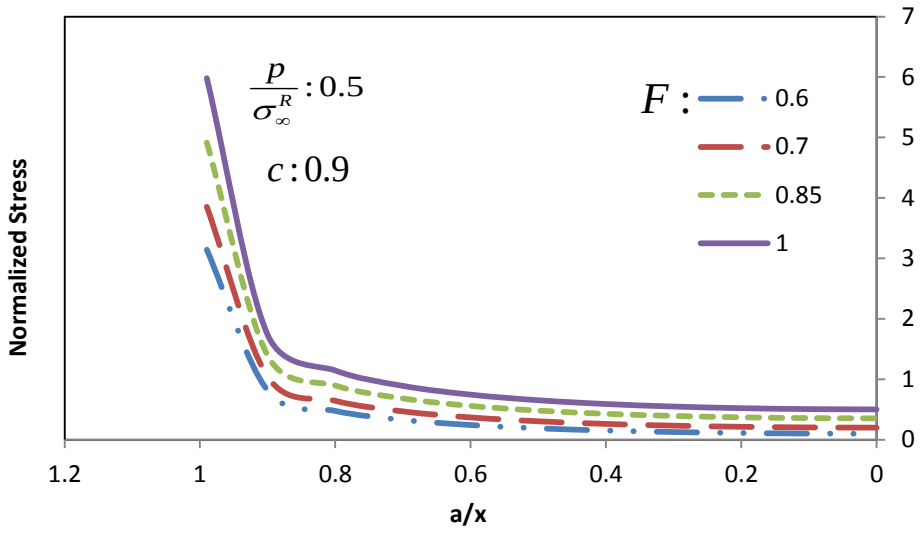

(a)

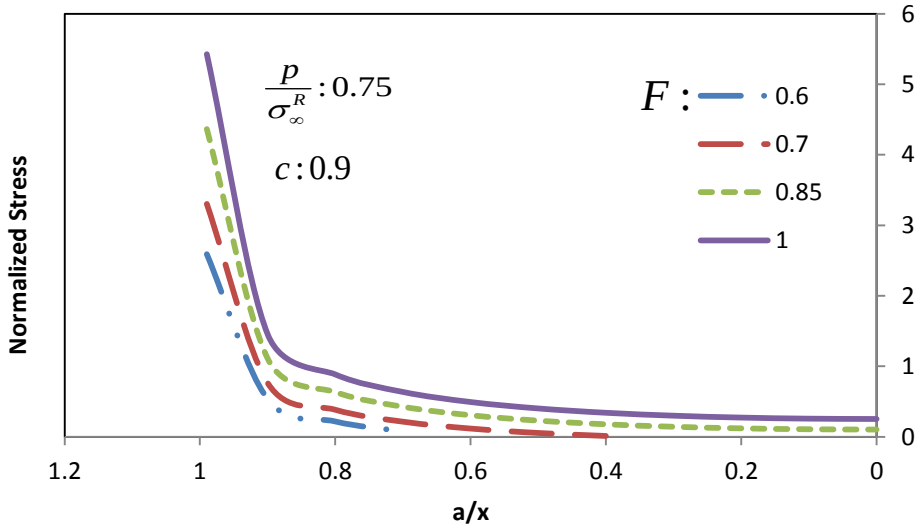

(b)

Figure 26: Effect of loading-unloading scenario on stress field- constant value of c and variable value of $\frac{p}{\sigma_\infty^R}$.

In Figure, the value of $\frac{p}{\sigma_{\infty}^{R}}$ remains constant and the effect of change in the value of c is considered. Comparing Figure(a) and Figure(b) shows that an increase in c results in an increase in the stress field. This phenomenon shows that larger bonding zone can have more reduction on the value of stress field.

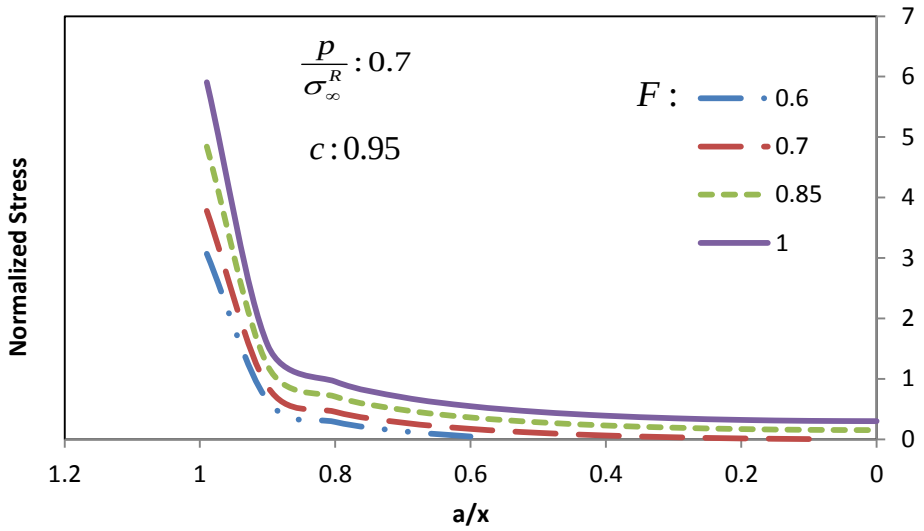

(a)

Figure 27: Effect of loading-unloading scenario on stress field- constant value of $\frac{p}{\sigma_{\infty}^{R}}$ and variable value of c.

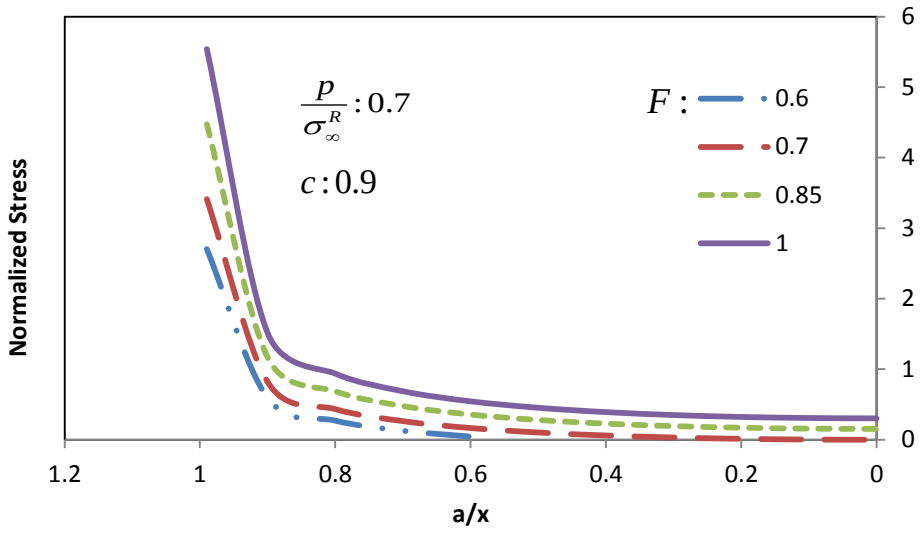

(b)

Figure 27: Continued.

4.3.4 Elastic media- Time-dependent bond strength

Since the bonding strength for this case is dependent on time and is independent of space, it does not affect Eq. (30). Therefore the result presented in Eq. (117) and (119) can be used for this case. The only difference that must be applied is substituting the time-dependent value of stress with the constant value of stress in Eq.(117) and (119). Eqs. (122) and (124) express the displacement and stress field for this case, respectively.

$$u_2 = \frac{k+1}{4G}\sigma_\infty^R\sqrt{a^2-x^2} - \frac{k+1}{4G}p(t)\sqrt{a^2-x^2} + \frac{k+1}{4G}\frac{2p(t)}{\pi}\left(\arcsin(c)\sqrt{a^2-x^2} - x\times\arctan\left(\frac{c}{\sqrt{1-c^2}}\frac{\sqrt{a^2-x^2}}{x}\right) + ac\times\arctan\left(\frac{1}{\sqrt{1-c^2}}\frac{\sqrt{a^2-x^2}}{a}\right)\right) \quad (122)$$

The displacement field is written in dimensionless format as follows,

$$\frac{u_2}{\frac{k+1}{4G}a\sigma_\infty^R}=\sqrt{1-(\frac{x}{a})^2}-\frac{p(t)}{\sigma_\infty^R}\sqrt{1-(\frac{x}{a})^2}+$$

$$\frac{2}{\pi}\frac{p(t)}{\sigma_\infty^R}(\arcsin(c)\sqrt{1-(\frac{x}{a})^2}-\frac{x}{a}\times\arctan(\frac{c}{\sqrt{1-c^2}}\frac{\sqrt{1-(\frac{x}{a})^2}}{\frac{x}{a}})+ \tag{123}$$

$$c\times\arctan(\frac{1}{\sqrt{1-c^2}}\sqrt{1-(\frac{x}{a})^2}))$$

$$\sigma_{22}=\frac{\sigma_\infty^R x}{\sqrt{x^2-a^2}}-\frac{p(t)x}{\sqrt{x^2-a^2}}+\frac{2p(t)x}{\pi\sqrt{x^2-a^2}}\arcsin(\frac{a-\beta}{a})- \tag{124}$$

$$\frac{2p(t)}{\pi}\arctan(\frac{(a-\beta)\sqrt{x^2-a^2}}{x\sqrt{2a\beta-\beta^2}})$$

$$\frac{\sigma_{22}}{\sigma_\infty^R}=\frac{1}{\sqrt{1-(\frac{a}{x})^2}}-\frac{p(t)}{\sigma_\infty^R}\frac{1}{\sqrt{1-(\frac{a}{x})^2}}+\frac{2}{\pi}\frac{p(t)}{\sigma_\infty^R}(\frac{1}{\sqrt{1-(\frac{a}{x})^2}}\arcsin(c)- \tag{125}$$

$$\arctan(\frac{c\sqrt{1-(\frac{a}{x})^2}}{\sqrt{1-c^2}}))$$

Wool and O'Connor (1982; 1981) formulate the traction stress shown in Eq.(126). k is dependent on temperature, pressure and molecular weight. When all the necessary chain ends are available for immediate reputation across the interface (no surface rearrangement) then $\dot{\psi}(t)=\delta(t)$ and Eq. (126) is changed into Eq. (127).

$$\sigma_b=\sigma_0+k't^{1/4}*\dot{\psi}(t) \tag{126}$$

$$\sigma_b=\sigma_0+k't^{1/4} \tag{127}$$

Instead of using Eq.(127), Eq. (82) is used in substituting $p(t)$. It is also assumed that the $\sigma_0=0.3\sigma_b(t_\infty)$ (Bhasin et al., 2008). As mentioned before, the left-hand side of

Eq. (123) is called normalized displacement. Figure 28 shows the effect of time-dependent bonding strength on normalized displacement. It is evident that an increase in time results in a decrease in displacement value in general. Comparing Figure 28(a) and Figure 28(b) illustrates that as the ultimate bonding strength increases, the normalized displacement decreases.

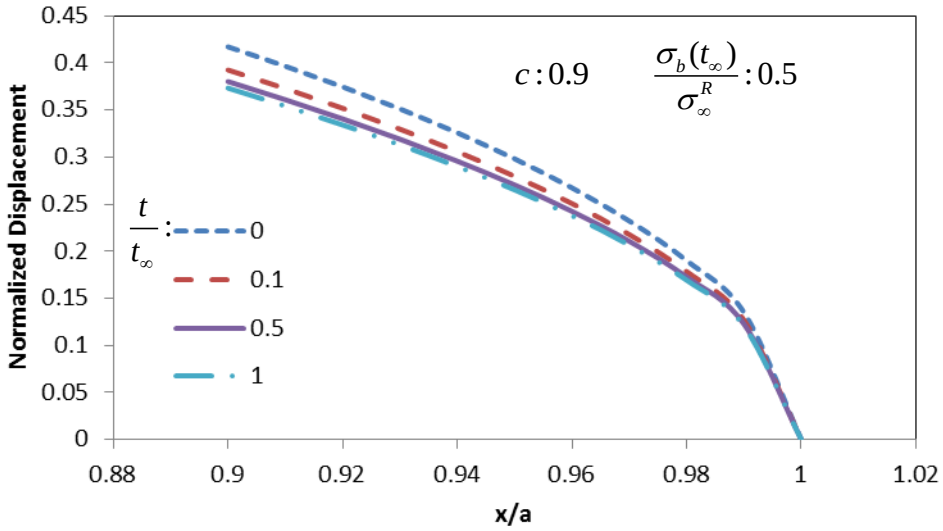

(a)

Figure 28: Effect of time-dependent bonding strength on normalized displacement-constant value of c and variable value of $\frac{\sigma_b(t_\infty)}{\sigma_\infty^R}$.

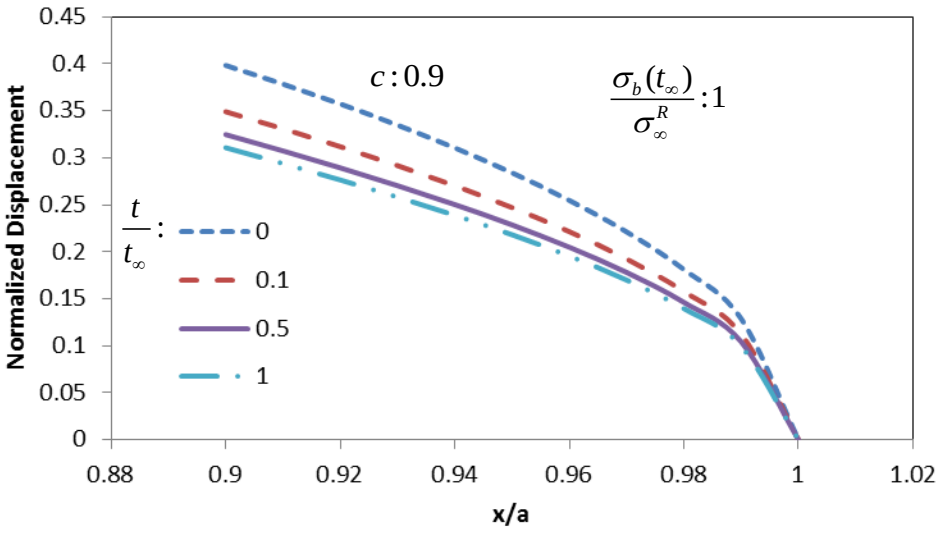

(b)

Figure 28: Continued.

In Figure 29, the effect of different bonding zone value of normalized displacement is evaluated. The greater bonding zone results in an decrease in the displacement value in $0.95 < \frac{x}{a} < 1$. In order to make this result more clear, Figure 29(c) shows the difference in the value of normalized displacement obtained from Figure 29(a), denoted by NU (33a) and Figure 29(b), denoted by NU(33b).

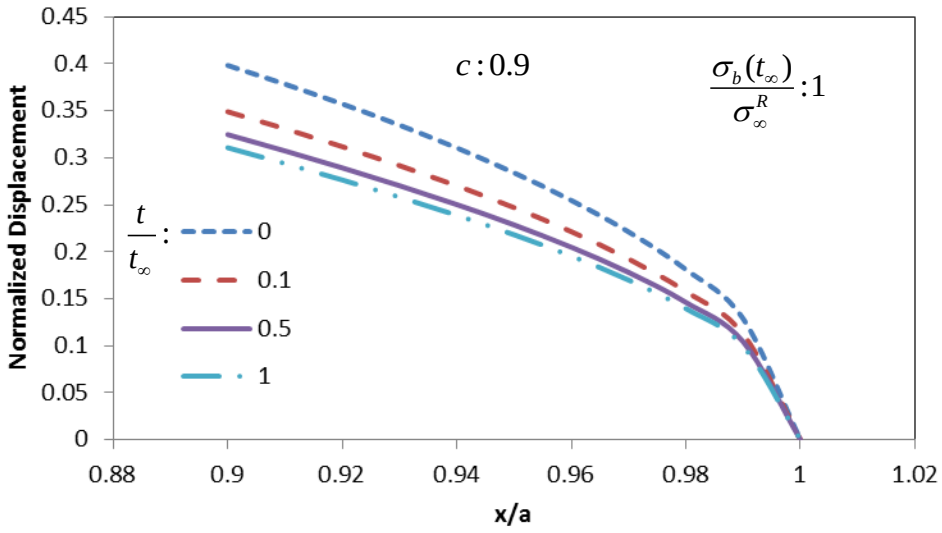

(a)

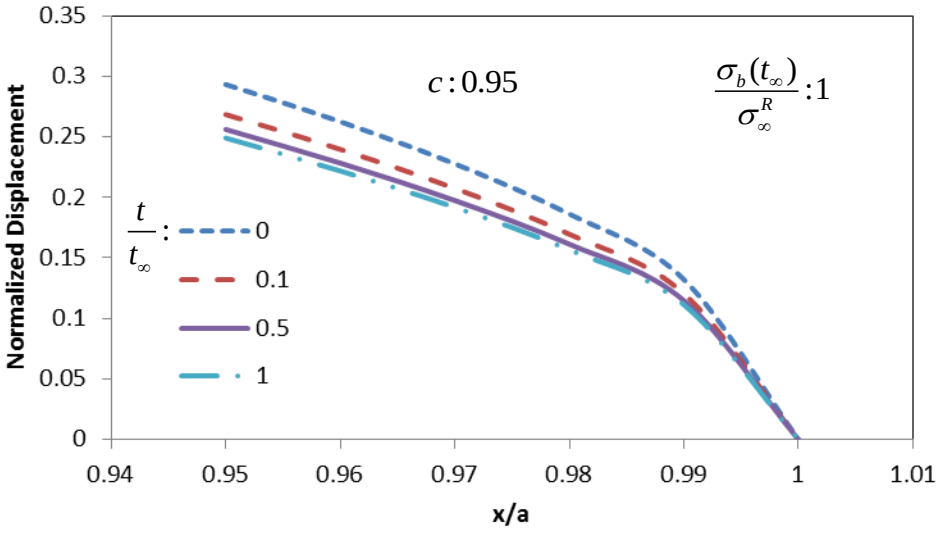

Figure 29: Effect of time-dependent bonding strength on normalized displacement- constant value of $\frac{\sigma_b(t_\infty)}{\sigma_\infty^R}$ and variable value of .

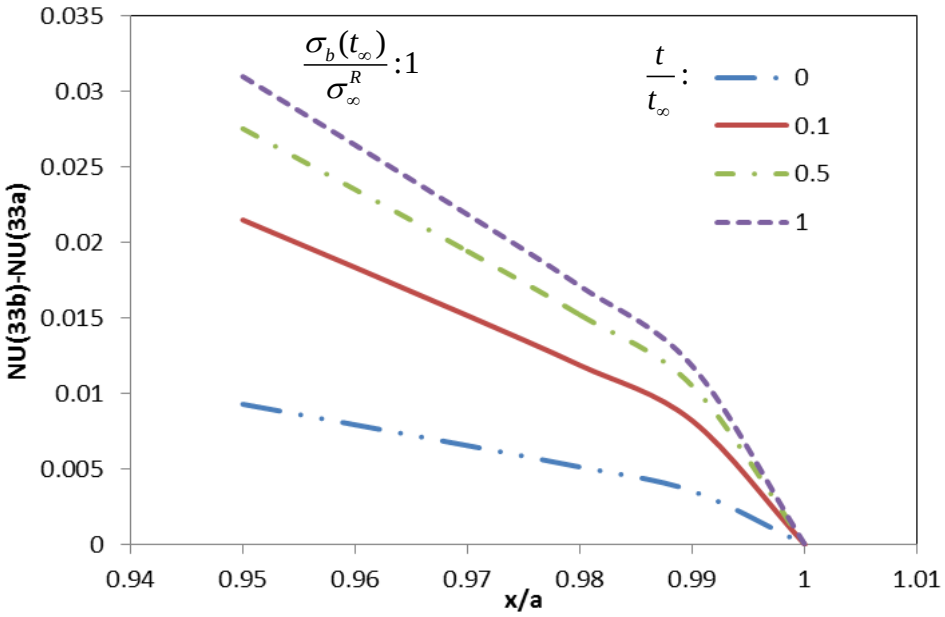

(c)

Figure 29: Continued.

Figure 30 shows the effect of time-dependent bonding strength on the normalized stress. It is clear that as time passes, the increasing bonding strength reduce the value of normalized stress. Moreover, as the ultimate value for bonding strength increase, the normalized stress decreases.

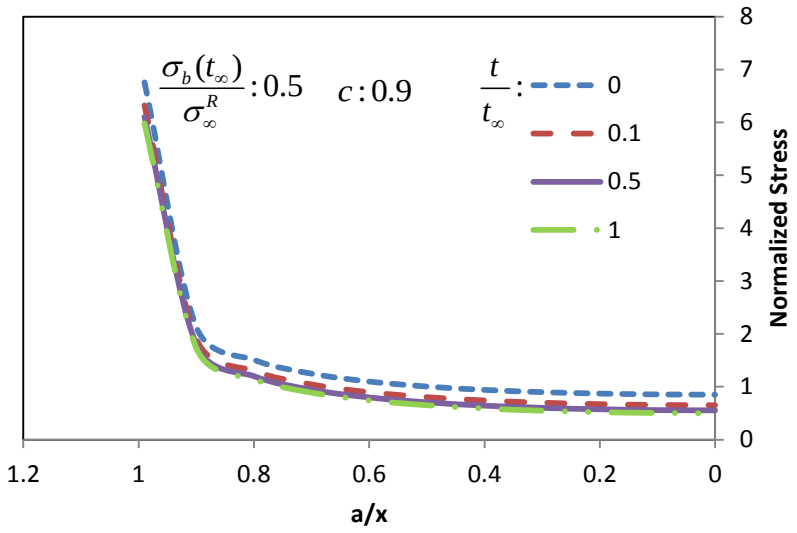

(a)

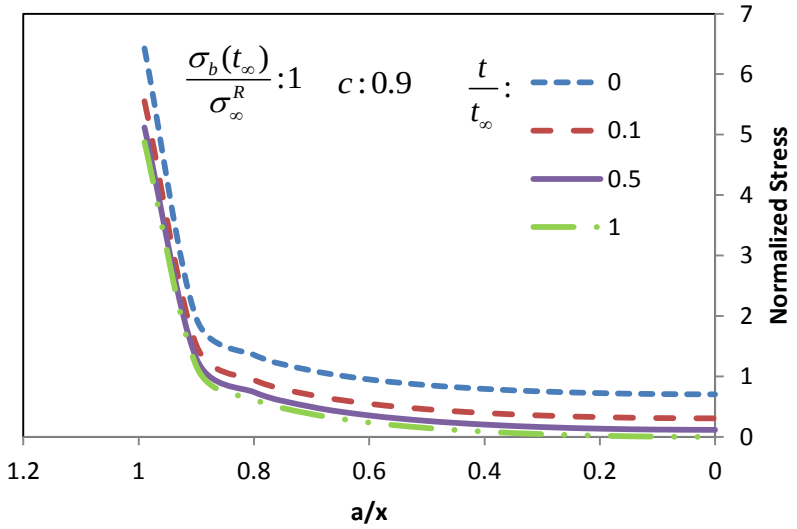

Figure 30: Effect of time-dependent bonding strength on normalized stress- constant value of $\frac{\sigma_b(t_\infty)}{\sigma_\infty^R}$ and variable value of c.

Figure 31 also illustrate the effect of bonding zone on the normalized stress. As expected, larger bonding zone has more impact on the reduction of normalized stress.

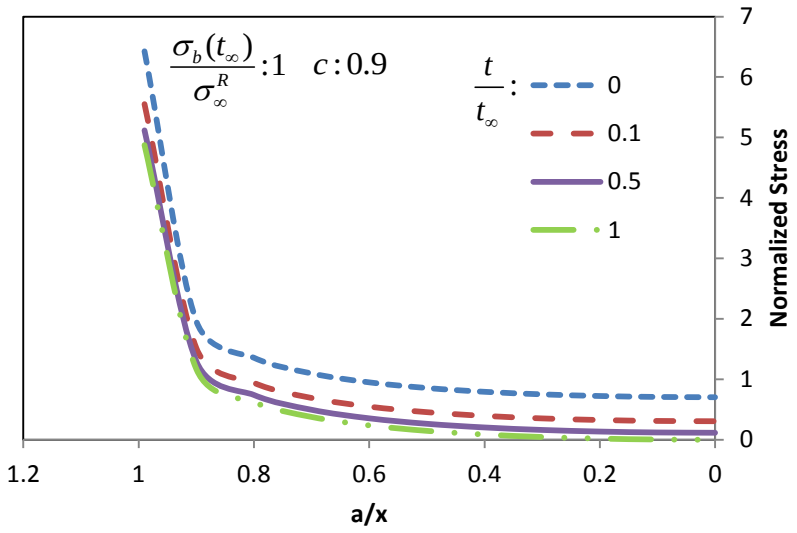

(a)

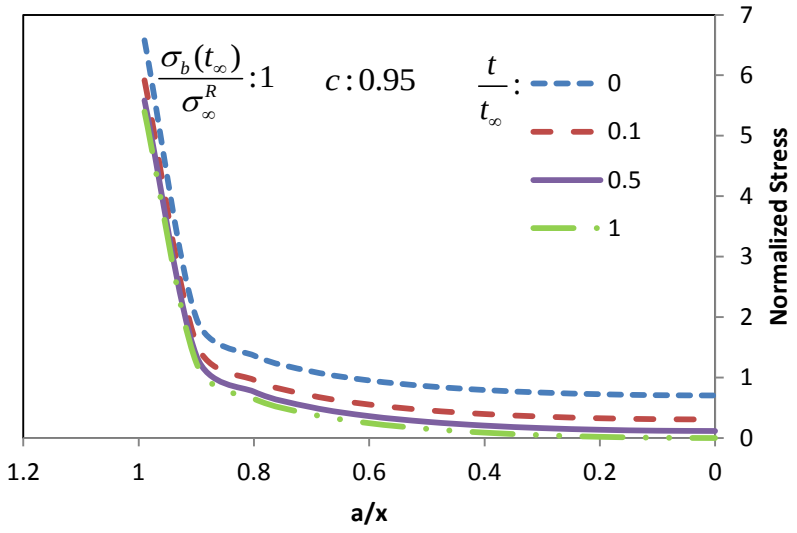

(b)

Figure 31: Effect of time-dependent bonding strength on normalized stress- constant value of c and variable value of $\frac{\sigma_b(t_\infty)}{\sigma_\infty^R}$.

4.3.5 Viscoelastic media

Time-independent bonding strength is the simplest case which can be argued. As discussed in the third correspondence principle, which is applicable for our case, the displacement field in elastic and viscoelastic media is the same. Considering constant bonding strength, Eq. (44) becomes easier to solve; however, time-independent bonding strength is not compatible with the true nature of the healing process. Using the convolution integral, the corresponding bonding strength in the viscoelastic media begins to relax, which contradicts the increasing nature of bonding strength with time. Moreover, Schapery assumed that bonding stress (σ_b^{VE}) is independent of time meaning that the healing phenomenon happens instantaneously between two surfaces, and the effect of long term healing is neglected in his work. The first step toward enhancing the work of Schapery to asphalt, is to use the work of Wool and O'Conner to model the long term effect of healing. Therefore instead of constant bonding strength, calculations start with time-dependent bonding strength in elastic media.

The effect of two parameters (i.e., m and λ) on the stress field is studied. First, a general formulation is considered for bonding strength instead of using Eq. (127) as expressed in Eq.(128).

$$\sigma_b^R(t) = \sigma_0 + k't^m \tag{128}$$

where $0 < m < 1$. Three different values, 0.25, 0.5 and 0.75 are selected for m. Second, two different values of 0.005 and 0.05 are chosen for λ (Zhang and Greenfield, 2007) in the relaxation modulus, which is expressed in Eq. (129)

$$E(t) = E_\infty + (E_0 - E_\infty)\exp(-\lambda t) \tag{129}$$

where $\lambda = \frac{1}{T_r}$ in which T_r is the relaxation time.

Using Eqs. (127), (44), and (129) the stress in Viscoelastic media is expressed as:

$$\sigma_b^{VE} = \{Ed\sigma_b^R\} = \frac{1}{E_R}\int_{0^-}^{t} E(t-\tau)\frac{d\sigma_b^R}{d\tau}d\tau =$$

$$\frac{1}{E_R}E(t)\sigma_0 + \frac{1}{E_R}E_\infty k' t^m + \exp(-\lambda t)\int_{0^+}^{t}\frac{E_0 - E_\infty}{E_R}\exp(\lambda\tau)mk'\tau^{m-1}d\tau = \quad (130)$$

$$\frac{1}{E_R}E(t)\sigma_0 + \frac{1}{E_R}E_\infty k' t^m + \frac{E_0 - E_\infty}{E_R}k'(m\exp(-\lambda t)\int_{0^+}^{t}\exp(\lambda\tau)\tau^{m-1}d\tau)$$

The first term in Eq. (130) shows relaxation in instantaneous healing. The second term indicates an increase in the value of bonding strength due to the time-dependent part of bonding stress. Eventually, this term reaches an asymptotic value of $\frac{1}{E_R}E_\infty k' {t_\infty}^m$ where t_∞ represents the time during which healing phenomenon is completed. Finally, the third component illustrates the coupling effect of recovery and relaxation. Further explanation is needed for the third part of Eq. (130). The integral in the third part was calculated by a Matlab code. The time increment, considered in Matlab code, is 10^{-5}. The difference between the results obtained based on different time increment (i.e. 10^{-5} and 10^{-6}) was less than 2 percent. Therefore, in order to reduce the calculation time, the smaller time increment was selected. For the simplicity of the figures, the value of $m\exp(-\lambda t)\int_{0^+}^{t}\exp(\lambda\tau)\tau^{m-1}d\tau$ is defined by $P\sigma 3$ (part of the 3rd component of stress). If sufficient time is given to the material with a long relaxation time, the value of $P\sigma 3$ will eventually reach 0.

An increase in the value of m directly results in an increase in bonding strength, which can be clearly seen in Figure 32. Moreover, an increase in the value of λ (a decrease in the value of relaxation time) has a negative effect on $P\sigma 3$. The corresponding time for the peak value of $P\sigma 3$ gets smaller with a decrease in relaxation time (i.e., the material starts to relax in a shorter period of time and therefore the value of bonding strength drops in a shorter period of time).

Moreover, λ changes with temperature. Hotter weather accelerates the process of relaxation. Therefore the relaxation time decreases, which results in an increase in λ value. It also matches the experimental result which shows that higher temperature accelerates the process of healing.

Another important contribution of this calculation is its ability to predict an optimum resting time for which the maximum bond strength can be obtained. The time at which the peak value of $P\sigma 3$ is occurred for each temperature is the optimum value for rest periods in that specific temperature because the maximum bond strength can be gained in this case. Therefore the optimum time for rest periods can be found using Figure 32.

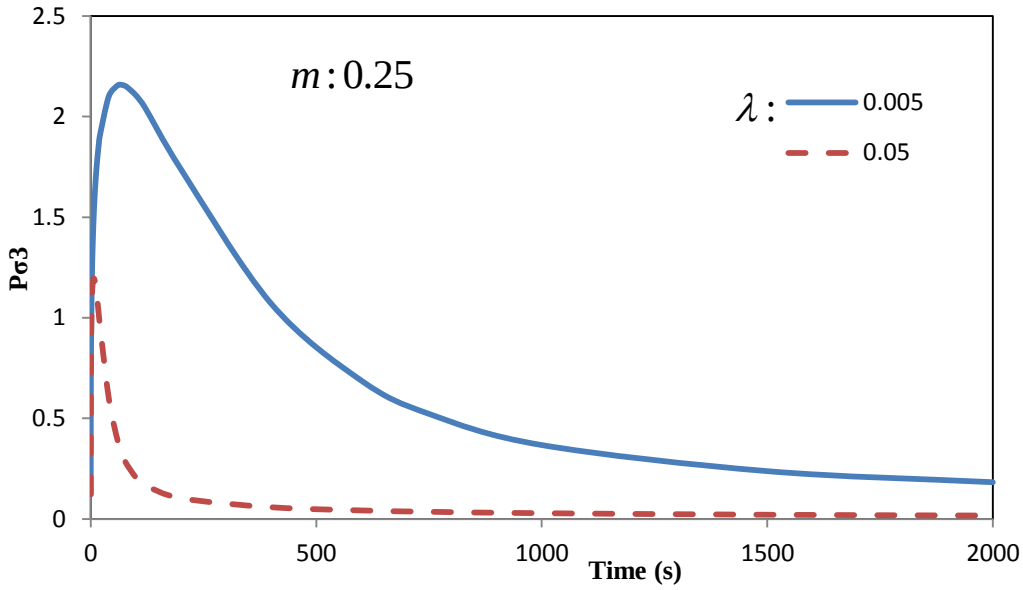

(a)

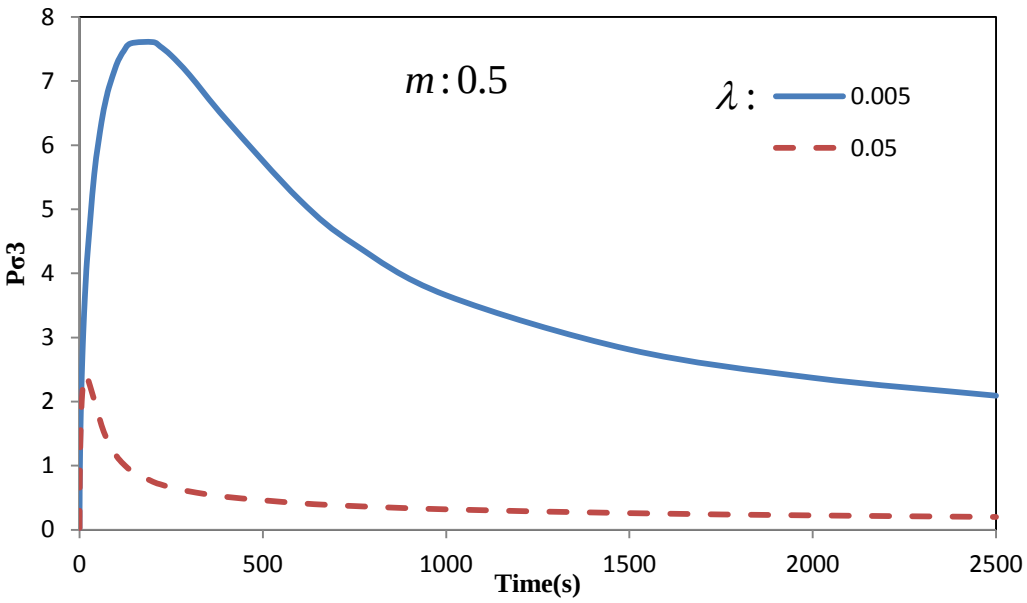

(b)

Figure 32: Effect of different values of m on $P\sigma 3$.

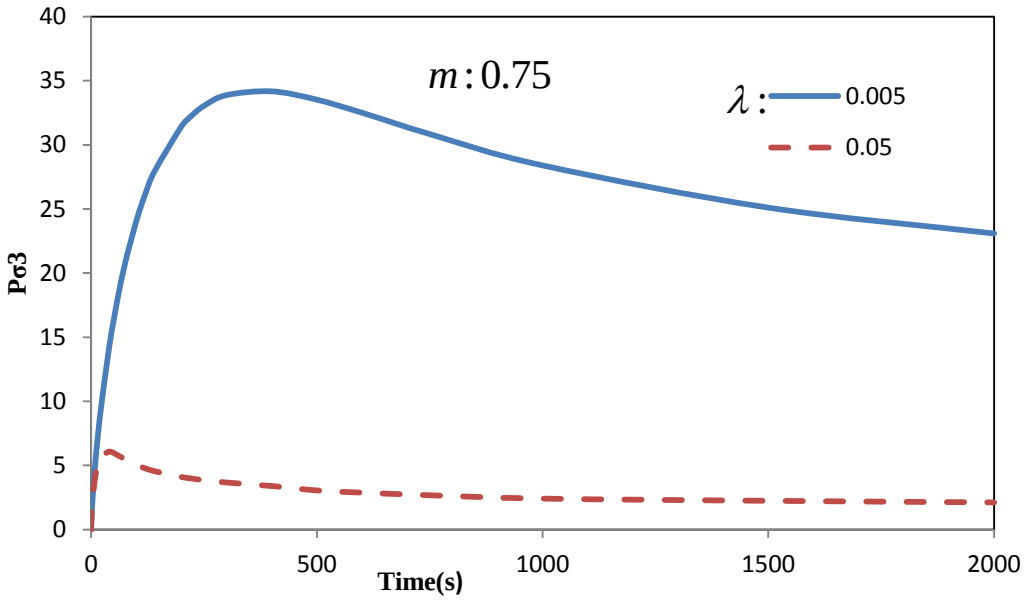

(c)

Figure 32: Continued.

Figure 33 shows the effect of different coefficient of bonding strength with a constant relaxation time. An increase in the value of bond strength leads to an increase in the stress field in the vicinity of the crack.

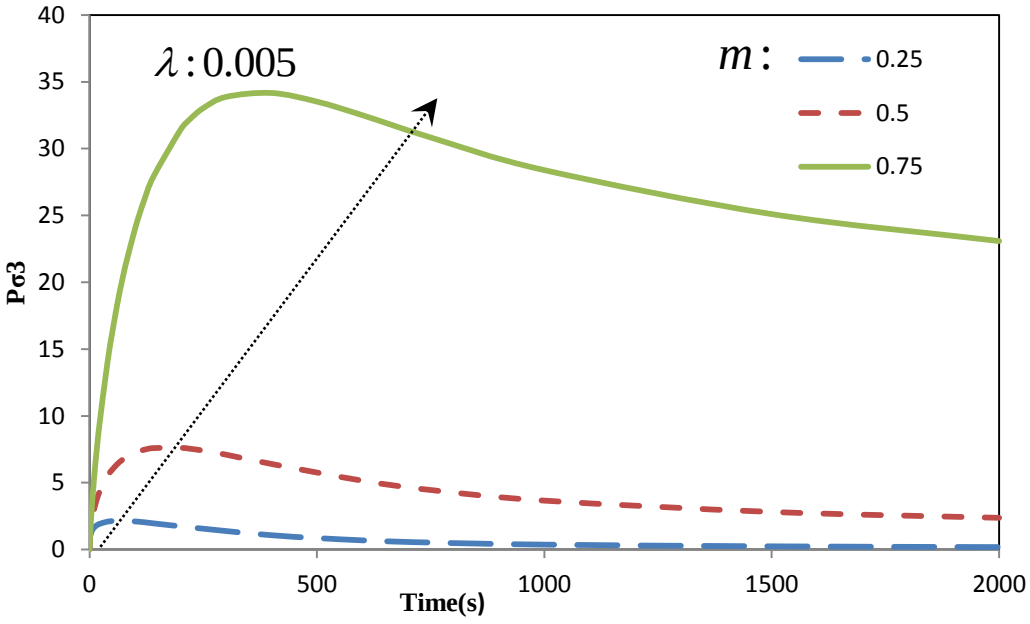

(a)

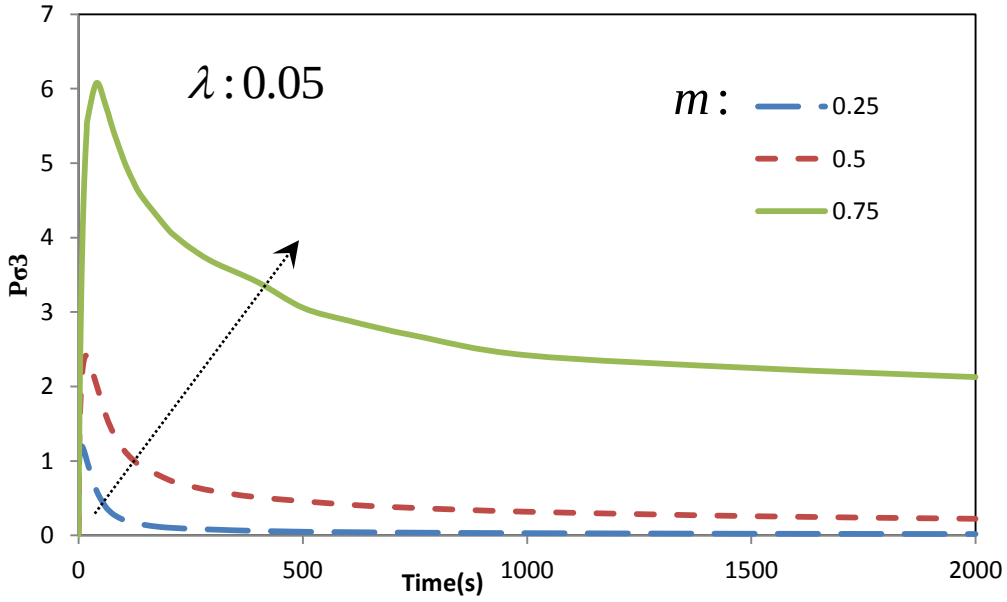

(b)

Figure 33: Effect of different values of λ on $P\sigma 3$.

The displacement field is also expressed in Eq.(131).

$$u_2 = \frac{k+1}{4G}\sigma_\infty^R\sqrt{a^2-x^2} - \frac{k+1}{4G}(\sigma_0 + k't^m)\sqrt{a^2-x^2} + \frac{k+1}{4G}\frac{2(\sigma_0 + k't^m)}{\pi}(\arcsin(c)\sqrt{a^2-x^2} - x*\arctan(\frac{c}{\sqrt{1-c^2}}\frac{\sqrt{a^2-x^2}}{x}) + ac*\arctan(\frac{1}{\sqrt{1-c^2}}\frac{\sqrt{a^2-x^2}}{a})) \quad (131)$$

Since the bonding zone is too small, constant bonding rate ($\dot{a}_b$) seems a reasonable assumption. Therefore time and displacement can transform into each other using $t = \frac{a-x}{\dot{a}_b}$.

The next step is to find the work done by the upper and lower parts of the crack.

$$W_b = \int u_2 \frac{d\sigma_b^{VE}(\tau)}{d\tau} d\tau \quad (132)$$

To obtain a solution for Eq. (132), numerical integration is needed, which remains a challenge for further study on this topic. By having the bonding work, bonding zone and the rate of bonding will be determined.

5. SUMMARY AND CONCLUSIONS

This section presents the pertinent conclusions regarding the analysis of the mechanisms of damage healing at the micro scale. These conclusions are followed by recommended directions for future work on this topic.

5.1 Summary of objectives and results

This thesis illustrates the effect of micro-damage healing on stress and displacement fields in the vicinity of a crack tip in a material, bitumen, which possesses self-healing potential. The micro-damage healing process is modeled by incorporating both instantaneous healing and time-dependent bond strength development between the crack faces. The time-dependent traction occurs in a small zone referred to as healing process zone. As a first approximation, of healing in bitumen, the effect of the micro-damage healing on crack propagation was investigated considering bitumen to perform as an elastic media by deriving analytical relations for Stress Intensity Factor (SIF) when micro-damage healing mechanisms are in effect. Rest periods have an impact on both bonding strength and bonding size. Longer rest periods result in larger healing process zones and greater values of bonding strength. The bonding forces between the upper and lower parts of the crack try to close the opening and therefore, an increase in the bonding strength results in a decrease in the value of SIF. It is also evident that, in order to reach a specific crack opening, the ultimate stress applied at the far field is required to be greater in order to propagate the crack with healing capability compared to the material

without this property. Referring to the aforementioned results, SIF is a way to quantify the impact of healing in elastic media.

In order to clearly capture healing phenomenon, a novel technique based on complex variables was used to derive the equations required to calculate the stress and displacement fields in elastic media. Using Schapery's third correspondence principle, which is suitable for analyzing the crack shortening (healing phenomenon), the corresponding results of stress and displacement fields in elastic media are converted into viscoelastic media. In this part of the thesis the impact of rest periods and loading-unloading scenario on healing were evaluated.

5.2 Conclusions

1. An increase in the bonding strength and healing process size results in a decrease in the both displacement and stress fields.
2. Loading-unloading scenarios play an important role in the phenomenon of healing. A decrease in the far field stress in the unloading part has the same impact as an increase in the bonding strength. The results obtained by the complex- variable method indicate that an increase in bonding strength and healing process zone will result in a decrease in the stress and displacement fields near the crack field.
3. The coefficient that defines the bonding strength and relaxation time in visco elastic media is a critical factor. An increase in the value of m (healing exponent) directly increases the bonding strength. Moreover, an increase in the value of λ (i.e., a decrease in the value of relaxation time) has a negative

effect on $P\sigma 3$ (a part of stress field in the vicinity of the crack in the visco elastic media which indicates the coupling of healing and relaxation). The corresponding time for the peak value of $P\sigma 3$ gets smaller with a decrease in relaxation time and therefore the value of bonding strength drops in a shorter period of time.

4. Hotter weather accelerated the process of relaxation. Another important contribution of stress field calculations in viscoelastic media is their ability to predict effective, economical and optimal rest periods. The corresponding rest period duration for peak value of $P\sigma 3$ for a respective temperature is associated with the period of time required to mobilize the maximum bond strength for the associated temperature.

5.3 Possible future work

Every model has its own advantages and disadvantages. The model presented in this thesis captures the effect of both instantaneous and intrinsic healing; however, it is based on mathematical calculations that require further validation for applicability of asphalt binders and mixtures and calibration for accuracy of prediction. Possible fruitful future research includes.

1. Identify a testing protocol to validate the accuracy and precision of the model.
2. Implement the calculations in ABAQUS with a cohesive zone element. In this case healing phenomenon is modeled and the results obtained from this method and mathematical calculations can be compared.

3. Expand the SIF analysis for elastic media to energy release rate for visco elastic media, which more realistically represent bitumen and asphalt mixtures.

REFERENCES

Abu Al-Rub, R.K., Darabi, M.K., Little, D.N., Masad, E.A., 2010. A micro-damage healing model that improves prediction of fatigue life in asphalt mixes. International Journal of Engineering Science 48, 966-990.

Barenblatt, G., 1959a. Equilibrium cracks formed during brittle fracture rectilinear cracks in plane plates. Journal of Applied Mathematics and Mechanics 23, 1009-1029.

Barenblatt, G.I., 1959b. The formation of equilibrium cracks during brittle fracture. General ideas and hypotheses. Axially-symmetric cracks. Journal of Applied Mathematics and Mechanics 23, 622-636.

Barenblatt, G.I., 1962. The mathematical theory of equilibrium cracks in brittle fracture, in: H.L. Dryden, T.v.K.G.K.F.H.v.d.D., Howarth, L. (Eds.), Advances in Applied Mechanics. Academic Press, United States, 55-129.

Bhasin, A., Little, D.N., Bommavaram, R., Vasconcelos, K., 2008. A framework to quantify the effect of healing in bituminous materials using material properties. Road Materials and Pavement Design 9, 219-242.

Bommavaram, R.R., Bhasin, A., Little, D.N., 2009. Determining intrinsic healing properties of asphalt binders. Transportation Research Record: Journal of the Transportation Research Board 2126, 47-54.

Broek, D., 1986. Elementary engineering fracture mechanics. Kluwer Academic Publishers Group, Netherlands.

Darabi, M.K., Abu Al-Rub, R.K., Little, D.N., 2012. A continuum damage mechanics framework for modeling micro-damage healing. International Journal of Solids and Structures 49, 492-513.

De Gennes, P.G., 1971. Reptation of a polymer chain in the presence of fixed obstacles. The Journal of Chemical Physics 55, 572-579.

Dugdale, D., 1960. Yielding of steel sheets containing slits. Journal of the Mechanics and Physics of Solids 8, 100-104.

Findley, W.N., Lai, J.S., Onaran, K., 1989. Creep and relaxation of nonlinear viscoelastic materials: with an introduction to linear viscoelasticity. Dover Publications, United States.

Griffith, A.A., 1921. The phenomena of rupture and flow in solids. Philosophical Transactions of the Royal Society of London. Series A, Containing Papers of a Mathematical or Physical Character 221, 163-198.

Hellan, K., 1985. Introduction to fracture mechanics. McGraw-Hill, United States.

Irwin, G.R., 1957. Analysis of stresses and strains near the end of a crack traversing a plate. Journal of Applied Mechanics 24, 361-364.

Kachanov, L., 1958. Time of the rupture process under creep conditions. Isv. Akad. Nauk. SSR. Otd Tekh. Nauk 8, 26-31.

Kim, Y.H., Wool, R.P., 1983. A theory of healing at a polymer-polymer interface. Macromolecules 16, 1115-1120.

Kim, Y.R., 2003. Fatigue and healing characterization of asphalt mixtures. Journal of Materials in Civil Engineering 15, 75-83.

Kim, Y.R., Little, D.N., Benson, F.C., 1990. Chemical and mechanical evaluation on healing mechanism of asphalt concrete (with discussion). Journal of the Association of Asphalt Paving Technologists 59, 240-275.

Kim, Y.R., Little, D.N., Lytton, R.L., 2001. Evaluation of microdamage, healing, and heat dissipation of asphalt mixtures, using a dynamic mechanical analyzer. Transportation Research Record: Journal of the Transportation Research Board 1767, 60-66.

Little, D.N., Bhasin, A., 2007. Exploring mechanism of healing in asphalt mixtures and quantifying its impact. Springer Series in Materials Science 100, 205-218.

Little, D.N., Lytton, R., Williams, D., Chen, C., 2001. Microdamage healing in asphalt and asphalt concrete, Volume I: Microdamage and microdamage healing, Project summary report.

Lytton, R., Chen, C., Little, D., 2001. Microdamage healing in asphalt and asphalt concrete, volume III: a micromechanics fracture and healing model for asphalt concrete, Project summary report.

Lytton, R.L., Uzan, J., Fernando, E.G., Roque, R., Hiltunen, D., Stoffels, S.M., 1993. Development and validation of performance prediction models and specifications for asphalt binders and paving mixes. Strategic Highway Research Program, Washington.

Mueller, H., 1971. Stress-intensity factor and crack opening for a linearly viscoelastic strip with a slowly propagating central crack. International Journal of Fracture Mechanics 7, 129-141.

Orowan, E., 1954. Energy criteria of fracture. Massachusetts Institute of Technology Cambridge.

Schapery, R., 1975. A theory of crack initiation and growth in viscoelastic media. International Journal of Fracture 11, 141-159.

Schapery, R., 1984. Correspondence principles and a generalizedJ integral for large deformation and fracture analysis of viscoelastic media. International Journal of Fracture 25, 195-223.

Schapery, R., 1989. On the mechanics of crack closing and bonding in linear viscoelastic media. International Journal of Fracture 39, 163-189.

Sedov, L., 1972. A course in continuum mechanics. Volume 4- Elastic and plastic solids and the formation of cracks(Book- A course in continuum mechanics. Volume 4- Elastic and plastic solids and the formation of cracks.). Groningen, Wolters-Noordhoff Publishing, 1972. 325.

Shen, S., Chiu, H.M., Huang, H., 2010. Characterization of fatigue and healing in asphalt binders. Journal of Materials in Civil Engineering 22, 846.

Tan, Y., Shan, L., Richard Kim, Y., Underwood, B.S., 2012. Healing characteristics of asphalt binder. Construction and Building Materials 27, 570-577.

Westergaard, H.M., 1939. Bearing pressure and cracks. Journal of Applied Mechanics 6, 49-53.

Williams, D., Little, D., Lytton, R., Kim, Y., Kim, Y., 2001. Microdamage healing in asphalt and asphalt concrete, volume II: laboratory and field testing to assess and evaluate microdamage and microdamage healing.

Williams, M., 1957. On the stress distribution at the base of a stationary crack. Journal of Applied Mechanics 24, 109-114.

Williams, M., 1959. The stresses around a fault or crack in dissimilar media. Bulletin of the Seismological Society of America 49, 199-204.

Wool, R., O'Connor, K., 1982. Time dependence of crack healing. Journal of Polymer Science: Polymer Letters Edition 20, 7-16.

Wool, R., Oconnor, K., 1981. A theory crack healing in polymers. Journal of Applied Physics 52, 5953-5963.

Zehnder, A., 2012. Fracture Mechanics. Springer, Netherlands.

Zhang, L., Greenfield, M.L., 2007. Relaxation time, diffusion, and viscosity analysis of model asphalt systems using molecular simulation. The Journal of Chemical Physics 127, 194502.